JOURNAL OF GEOPHYSICAL RESEARCH, VOL. 102, NO. B4, PAGES 8217-8243, APRIL 10, 1997

Oblique strike-slip faulting of the central Cascadia submarine forearc

Chris Goldfinger and LaVerne D. Kulm
College of Oceanic and Atmospheric Sciences, Oregon State University, Corvallis

Robert S. Yeats, Lisa McNeill, and Cheryl Hummon
Department of Geosciences, Oregon State University, Corvallis

Abstract. At least nine WNW trending left-lateral strike-slip faults have been mapped on the Oregon-Washington continental margin using sidescan sonar, seismic reflection, and bathymetric data, augmented by submersible observations. The faults range in length from 33 to 115 km and cross much of the continental slope. Five faults offset both the Juan de Fuca plate and North American plates and cross the plate boundary with little or no offset by the frontal thrust. Left-lateral separation of channels, folds, and Holocene sediments indicate active slip during the Holocene and late Pleistocene. Offset of surficial features ranges from 120 to 900 m, and displaced subsurface piercing points at the seaward ends of the faults indicate a minimum of 2.2 to 5.5 km of total slip. Near their western tips, fault ages range from 300 ka to 650 ka, yielding late Pleistocene-Holocene slip rates of 5.5 ± 2 to 8.5 ± 2 mm/yr. The geometry and slip direction of these faults implies clockwise rotation of fault-bounded blocks about vertical axes within the Cascadia forearc. Structural relationships indicate that some of the faults probably originate in the Juan de Fuca plate and propagate into the overlying forearc. The basement-involved faults may originate as shears antithetic to a dextral shear couple within the slab, as plate-coupling forces are probably insufficient to rupture the oceanic lithosphere. The set of sinistral faults is consistent with a model of regional deformation of the submarine forearc (defined to include the deforming slab) by right simple shear driven by oblique subduction of the Juan de Fuca plate.

Introduction

The anelastic response of forearcs to oblique subduction can be highly variable. The most commonly recognized form is arc-parallel strike-slip faulting. This type of strain partitioning has been recognized in Sumatra [*Fitch*, 1972; *Jarrard*, 1986; *McCaffrey*, 1991], the Kurils [*Kimura*, 1986], the Philippines [*Karig et al.*, 1986], South America [*Dewey and Lamb*, 1992], and other forearcs [*Beck*, 1983]. The Sumatran forearc translates along the arc-parallel Great Sumatran fault, with the slip rate controlled by convergence obliquity [*Fitch*, 1972; *Jarrard*, 1986; *McCaffrey*, 1991]. In Japan, the Median Tectonic Line (MTL) serves a similar role in the subduction of the Philippine Sea plate [*Fitch*, 1972; *Sangawa*, 1986]. The Aleutian arc exhibits both arc-parallel translation and rotation of obliquely oriented blocks about vertical axes [*Geist et al.*, 1988; *Ryan and Scholl*, 1993]. Both of these mechanisms are favored in oblique subduction because the high-angle faults concentrate horizontal shear more effectively than the dipping subduction interface [*Fitch*, 1972].

The Cascadia subduction zone consists of two small plates, the Gorda and Juan de Fuca (JDF), subducting to the northeast beneath the North American plate (NOAM) (Figure 1). The subduction system is bounded to the north and south by triple junctions and includes the smaller Explorer plate to the north, which may not be presently subducting [*Rohr and Furlong*, 1995]. JDF-NOAM convergence is estimated as 40 mm/yr, directed 062° at 45°N along the deformation front (rotation poles of *DeMets et al.* 1990]). No active arc-parallel faults equivalent to the MTL or Great Sumatran fault have been identified onshore in Cascadia. *Snavely* [1987] inferred that the Fulmar fault, a north striking dextral strike-slip fault, offsets the continental slope and outer shelf in Oregon by about 200 km and attributed an abrupt truncation of the basaltic Siletzia terrane to this fault (Figure 2). The Fulmar fault exhibits small offsets of Quaternary strata in southern Oregon but was mainly active in the Eocene [*Snavely*, 1987]. Some discontinuous arc-parallel faults have been identified in the Cascadia forearc, both onshore and offshore which may accommodate some northward translation of the Cascadia forearc (Figure 2) [*Weaver and Smith*, 1983; *Blake et al.*, 1985; *Niem et al.*, 1992; *Kelsey and Bockheim*, 1994; *Goldfinger*, 1994; *Goldfinger et al.*, 1992a].

Paleomagnetically determined clockwise rotations of coastal basalts in Oregon and Washington suggest that a process of dextral shear of the forearc has operated throughout the Tertiary. Miocene (12-15 Ma) Columbia River Basalts in western Oregon are rotated 10-30° clockwise, and Eocene Siletz River Volcanics are rotated up to 90° clockwise [*Wells and Heller*, 1988; *England and Wells*, 1991]. Mechanisms proposed to explain these rotations include microplate rotation during terrane accretion, basin and range extension, distributed small block rotation, or a combination of these (see *Wells and Heller* [1988] for summary).

Paper number 96JB02655.
0148-0227/97/96JB-02655$09.00

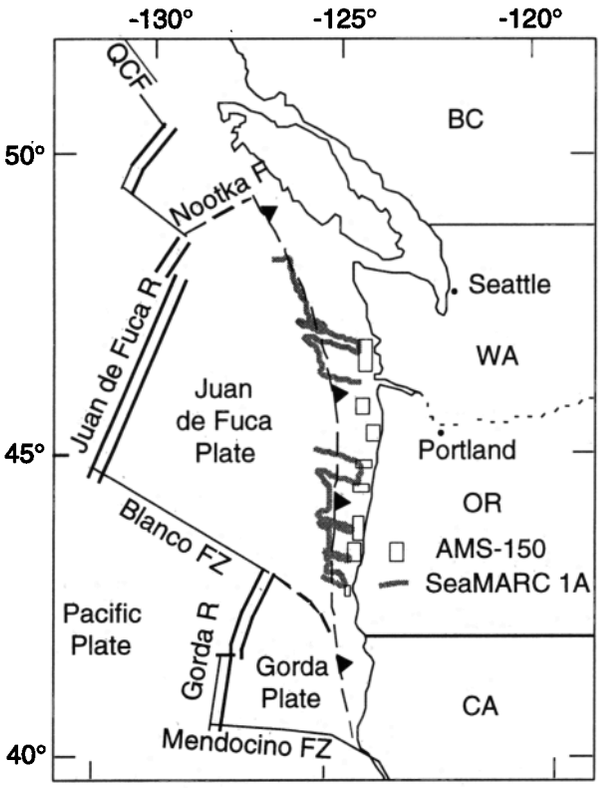

Figure 1. Tectonic map of the Cascadia subduction zone-Juan de Fuca plate system. Approximate SeaMARC 1A sidescan coverage from *Thomas Thompson* cruise TT 020 shown shaded, boxes indicate approximate Alpha Marine Systems (AMS) 150-kHz survey areas.

We have identified nine WNW trending transverse structures deforming the Cascadia accretionary prism off Oregon and Washington. Eight of these structures are left-lateral strike-slip faults based on measured offsets of surface and subsurface features. Five of the transverse faults can be traced across the plate boundary into the subducting Juan de Fuca plate, up to 21 km seaward of the deformation front. Documentation of these faults comes from sidescan sonar data, swath bathymetry, seismic reflection data, and field observations from submersibles. In this paper we summarize detailed surveys of these faults on the central Cascadia margin of Oregon and Washington and discuss their origin, structural significance, and implications for deformation of the submarine forearc.

Methods

Data Acquisition and Processing

High-resolution sidescan sonar data were collected with a deep-towed SeaMARC 1A 30-kHz system capable of imaging a 2-km or a 5-km swath width with spatial resolutions of 1 and 2.5 m, respectively. An Alpha Marine Systems (AMS) 150-kHz system was used to collect sidescan data on the continental shelves of Oregon and Washington, with a 1-km swath width and 0.5-m resolution. Approximate coverage of these surveys is shown in Figure 1. All sidescan data were located using Global Positioning System (GPS), then processed using Oregon State University's (OSU's) Sonar deep-tow sidescan processing system. Processing included towfish positioning, geometric and speed corrections, correction for towfish attitude, georeferencing of image pixels to a latitude-longitude grid, histogram equalization, and image enhancement. The final imagery was then integrated with other data layers in a raster/vector Geographical Information System (GIS) for analysis [*Goldfinger and McNeill*, 1996].

Regional sidescan data [*EEZ-SCAN 84 Scientific Staff*, 1986] using the (GLORIA) shallow-towed system were also used in interpretation of margin structure. The GLORIA imagery was georeferenced to Hydrosweep bathymetry collected by us in Washington (1993), or existing National Oceanic and Atmospheric Administration (NOAA) SeaBeam bathymetry in Oregon in order to produce a consistent spatial data set.

In our structural interpretations we have used about 30,000 km of seismic reflection profiles collected by academic institutions, the U.S. Geological Survey, NOAA, and the petroleum industry [*Goldfinger et al.*, 1992a]. The seismic reflection profiles vary widely in quality, depth of penetration, and navigation accuracy and range from single-channel sparker records navigated with LORAN A to 144-channel digital profiles navigated with GPS. An important data set is a multichannel seismic survey conducted off central Oregon in 1989 [*MacKay et al.*, 1992]. Approximately 2000 km of NAVSTAR-navigated 144-channel reflection profiles were collected and processed through time migration at the University of Hawaii. Three of the Oregon strike-slip faults intersect the deformation front within this survey (Figure 3), allowing detailed structural analysis, as well as determination of fault slip rates.

Fault Retrodeformation

The abundance of seismic and sidescan data allowed us to determine the slip rates on five transverse strike-slip faults on the Oregon and Washington margin. The method for slip rate determination is described here, as it is similar for all five faults. We utilized the simple geometry of trenchward thickening abyssal plain sediment wedges, as determined by at least one trench-parallel and two trench-normal reflection profiles adjacent to each strike-slip fault (Figure 4). If the geometry of the pre-faulting trenchward thickening wedges is simple: three profiles can define the wedge geometry sufficiently to use them as three-dimensional (3-D) piercing points, the offsets of which represents the net slip of the fault. The three Oregon faults used many more profiles than did the Washington faults, which had the minimum number of profiles needed. Reflection data indicate that the geometry of the wedges is simple; and the layers that bound them are approximately planar over the distances involved. *Goldfinger et al.* [1996a] also calculated the net slip of one fault (the Wecoma fault) using isopach plots of two subsurface units. Using the wedge geometry captures total offset by the fault, which often is underestimated in measurements of offset isopachs due to drag folding and local velocity effects near the fault. The five faults for which we used this technique have a vertical component of offset and show pronounced growth strata on the downthrown block; thus we were able to easily distinguish synfaulting and prefaulting units (Figure 3). We identified the point in the section at which interval thickness across the fault reversed from thicker on the downthrown block to thinner on the downthrown block. Synfaulting sedimentary units could not be used for this determination

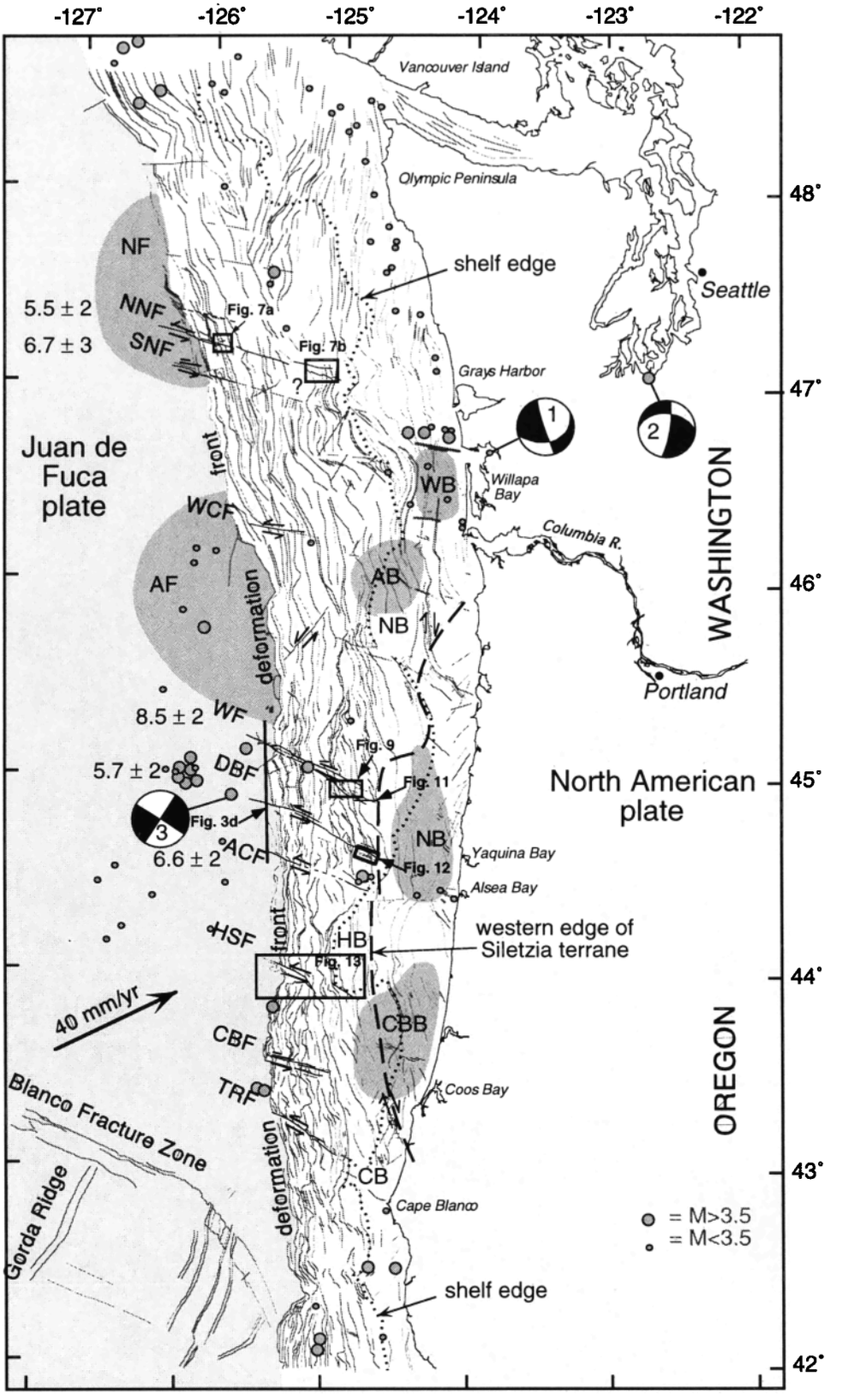

Figure 2. Active tectonic map of the Oregon-Washington continental margin. Faults and anticlines shown; synclines deleted for clarity. JDF-NOAM vector of *DeMets et al.* [1990] is shown. Siletzia terrane boundary based on magnetics and reflection-refraction data. Strike-slip faults shown with slip rates in mm/yr. NNF, North Nitinat fault; SNF, South Nitinat fault; WCF, Willapa Canyon fault; WF, Wecoma fault; DBF, Daisy Bank fault; ACF, Alvin Canyon fault; HSF, Heceta South fault; CBF, Coos Basin fault; TRF , Thompson Ridge fault. NF, Nitinat Fan; AF, Astoria Fan. Major depocenters are shown by stipple: WB, Willapa Basin; AB, Astoria Basin; NB, Newport Basin; CBB, Coos Bay Basin. Submarine Banks are NB, Nehalem Bank; HB, Heceta Bank; CB, Coquille Bank. All offshore seismicity is shown, with Blanco Fracture Zone and Gorda plate events removed. Focal mechanisms 1, 2, and 3, are M 3.3, M 7.1, and M 5.8 slab earthquakes, respectively, and are discussed in the text.

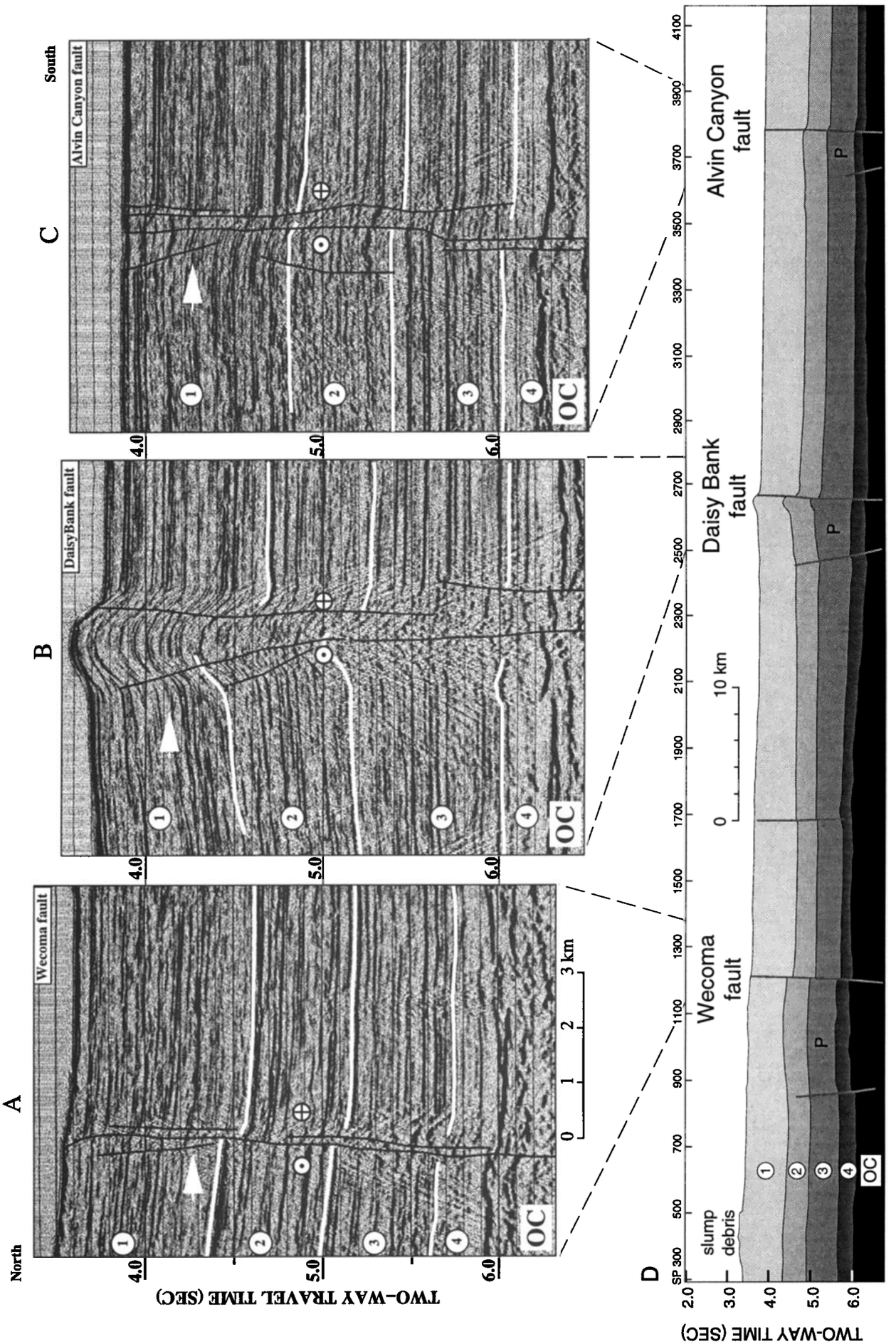
A
B
C
D
North
South
Wecoma fault
DaisyBank fault
Alvin Canyon fault
OC
0 1 2 3 km
TWO-WAY TRAVEL TIME (SEC)
4.0
5.0
6.0
SP 300 500 700 900 1100 1300 1500 1700 1900 2100 2300 2500 2700 2900 3100 3300 3500 3700 3900 4100
2.0
3.0
4.0
5.0
6.0
slump debris
Wecoma fault
Daisy Bank fault
Alvin Canyon fault
0 10 km
P
TWO-WAY TIME (SEC)

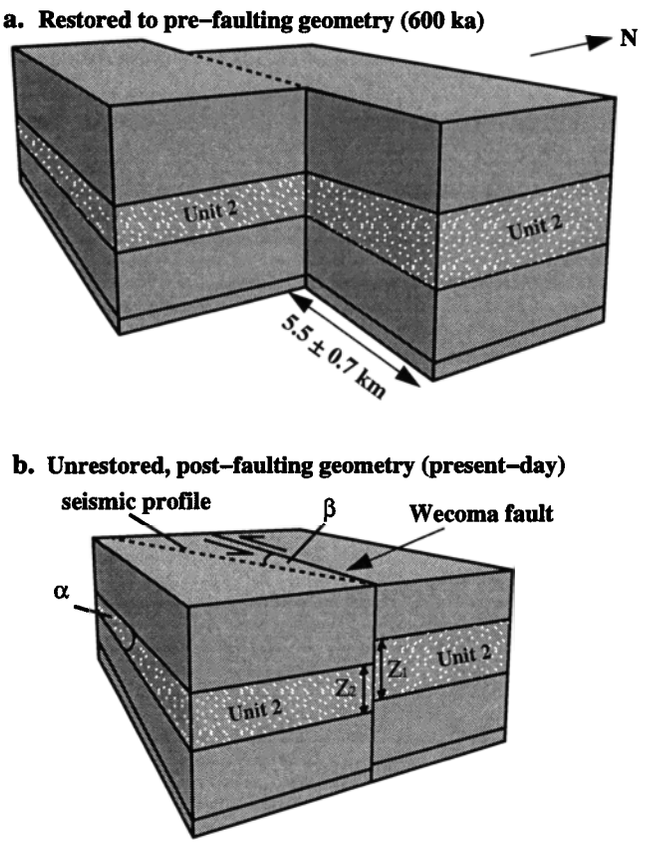

Figure 4. Cartoon diagram illustrating strike-slip fault restoration. (a) Abyssal plain section restored to prefaulting configuration (600 ka). (b) Unrestored section as imaged on MCS line 37 (present-day). The three-dimensional (3-D) wedge bounding units 2 and 3, as well as individual reflector-bound intervals within the units, form the 3-D piercing points which were matched across the fault to determine fault slip. Unit 2 resolved the fault offset somewhat better because it thickened more rapidly to the east than unit 3. Relation used to calculate net slip is given in the text. The variables used are shown here: α is the angle between the bounding reflectors of the principal seismic units and B is the angle between the strike of the seismic profile used in restoration, and the strike of the fault. Z_1 and Z_2 are thicknesses of the restored unit in the upthrown and downthrown blocks, respectively. Example is for the Wecoma fault.

because the presence of growth strata invalidates the assumption that measured geometric changes on the profiles result from horizontal fault offset only. In practice, we used two methods to determine fault slip. For all five faults, we determined the wedge geometry from the seismic grid, then determined the fault offset required to produce the observed thickness change for two pre-faulting units (units 2 and 3 in Figure 3). If Z_1 and Z_2 are the thicknesses of the offset unit across the fault, α is the angle between the bottom and top contacts of the unit (defining the eastward thickening wedge), and β is the plan view angle between the seismic profile and the fault, net fault slip (S) is then given by $S = [Z_1\text{-}Z_2/\tan\alpha]\cos\beta$. For the three Oregon faults, we also used a trial and error restoration using the reflection profiles directly. To find the best fit offset required to restore the abyssal plain geometry, we iteratively tested the offset to find the best match of between 10 and 18 individual reflectors within the prefaulting section using the margin-parallel and margin-normal reflection profiles and correcting for the difference between fault strike and profile strike (as with β above). The geometry used in both methods is illustrated schematically in Figure 4. The error estimate includes the minimum and maximum fault separation that could be accommodated within the interpretation of the seismic data.

We estimated the age of faulting by converting the two-way travel time to the base of the growth strata to depth in meters. This conversion used an average velocity of 1680 m/s, calculated for the upper 400 m of the Nitinat fan from Ocean Drilling Program (ODP) drilling and reflection data [*Hyndman and Davis*, 1992; *Shipboard Scientific Party*, 1994]. We derived fault age by using a net sedimentation rate of 100 cm/1000 years for the Nitinat fan calculated from the 1993 ODP drill sites [*Shipboard Scientific Party*, 1994] and 110 cm/1000 years for the Astoria fan [*Goldfinger*, 1994; *Goldfinger et al.*, 1996a] calculated using the thickness and age of the fan. To establish the age of the Astoria fan, we correlated a prominent seismic reflector at the base of the fan from the Wecoma fault to Deep Sea Drilling Project (DSDP) Site 174A (70 km southeast) using a seismic reflection profile connecting the drill site to the fault [*Kulm et al.*, 1973a, b; *Goldfinger et al.*, 1996a]. A profound lithologic change between sand turbidites of the fan and silt turbidites of the abyssal plain sequence was observed at the depth of this reflector in the drill cores. Biostratigraphic analysis of the cores from Site 174 yields an age of 760 ± 50 ka (J. C. Ingle, Stanford University, written communication, 1995). We infer that the age of the base of the fan is approximately the same at the Wecoma fault because we observe no significant onlap or offlap relationships within several hundred vertical meters of the base of the fan and the trend of the seismic section is subperpendicular to the sediment transport direction. Thus it is unlikely that significant time transgression has occurred between Site 174A and the Wecoma fault. For the other two Oregon faults (Daisy Bank and Alvin Canyon faults) we also use the base of the fan to estimate fault age, although it is likely to be slightly older due to the more southerly (distal) position of these faults. Although additional uncertainties exist in sedimentation rates, age of the fan, and seismic velocities, we use the same estimate of

Figure 3. The (a) Wecoma, (b) Daisy Bank, and (c) Alvin Canyon faults imaged on a N-S 144-channel migrated reflection profile (MCS line 37) approximately 3 km seaward of the deformation front. Seismic unit bounding reflectors used for fault restoration are shown in white. Base of growth strata is shown with white arrows. Growth strata thicken on the downthrown block; prefaulting units 2 and 3 thin on the downthrown block as a result of strike-slip motion. (d) Regional seismic reflection line showing the basement popup structures (P) that similarly offset oceanic crust at the three faults. Fourth fault under the kilometer scale is a tear fault in the sedimentary section only.

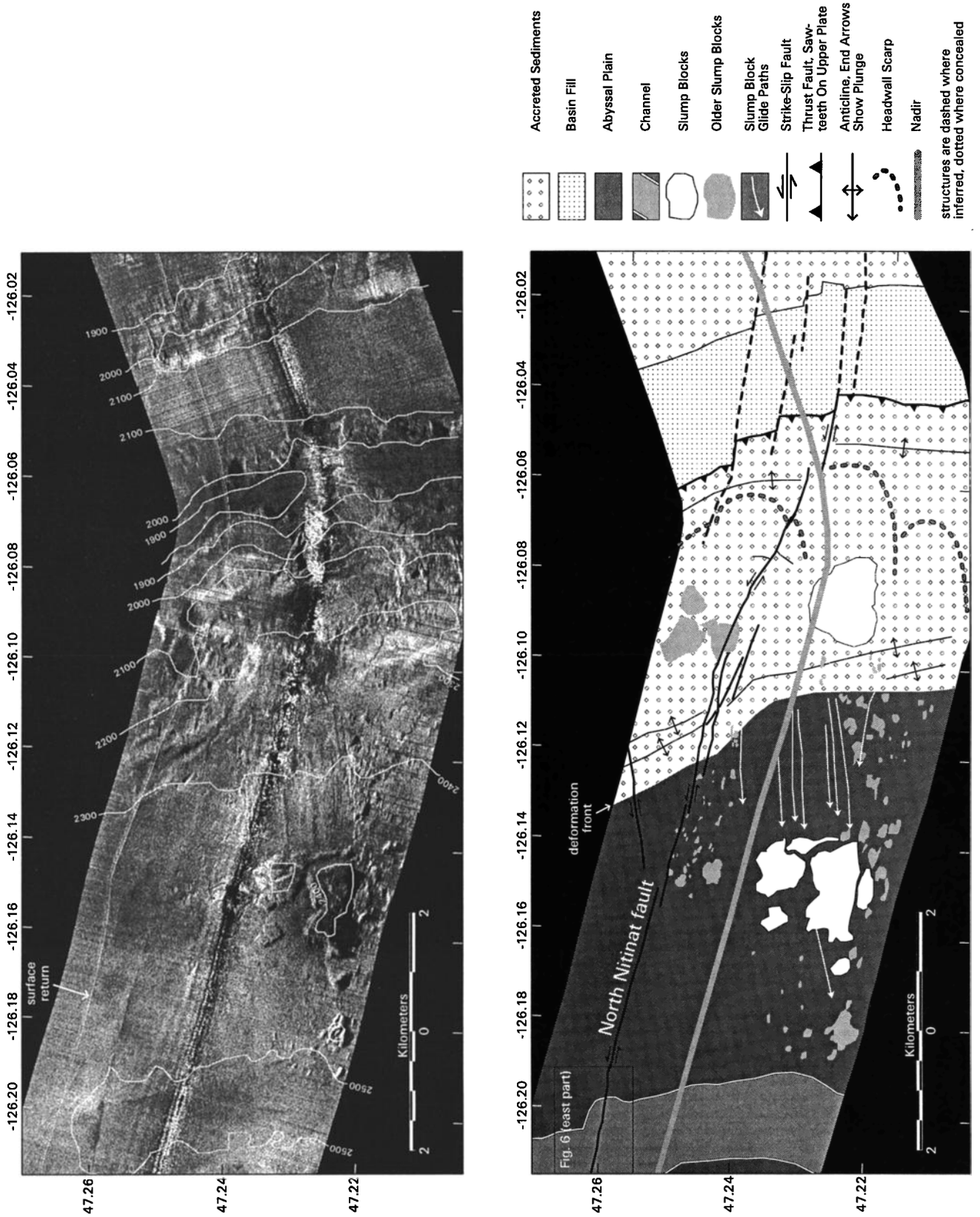
Accreted Sediments
Basin Fill
Abyssal Plain
Channel
Slump Blocks
Older Slump Blocks
Slump Block Glide Paths
Strike-Slip Fault
Thrust Fault, Saw-teeth On Upper Plate
Anticline, End Arrows Show Plunge
Headwall Scarp
Nadir
structures are dashed where inferred, dotted where concealed
surface return
deformation front
North Nitinat fault
Fig. 6 (east part)
Kilometers
-126.20
-126.18
-126.16
-126.14
-126.12
-126.10
-126.08
-126.06
-126.04
-126.02
47.26
47.24
47.22

error (± 50 kyr) here because we are unable to quantify these errors independently.

The age of the fault is then simply the depth in meters of the oldest growth strata, divided by the sedimentation rate in meters per 1000 years. The age of first vertical motion for each fault is calculated in this way, and the net slip can then be divided by the age to obtain the slip rate of the fault. Any pure strike-slip motion (no vertical component) that occurred prior to vertical displacement would result in an underestimate of the age of the fault, and thus our derived slip rate values will be too high.

In two cases (Wecoma and North Nitinat faults) we were able to calculate slip rates independently using measured offsets of late Pleistocene channels (120 m and 150 m, respectively) and estimated channel ages. Seismic reflection records showing the truncation of deep-sea channel walls and numerous sediment hiatuses in cores from the axial part of these channels document the erosive character of the coarse-grained late Pleistocene turbidity currents in this region [*Griggs and Kulm*, 1973]. We estimate the age of the offset channel walls to be 12-24 ka, consistent with incision during the last episode of high turbidity-current activity during the Wisconsin low stand [*Goldfinger et al.*, 1992a]. We assume fault motion was constant during the Holocene and late Pleistocene. Using this age range, we calculated a latest Pleistocene-Holocene slip rate of 8.3 ± 4 and 8.5 ± 4 mm/yr for the North Nitinat and Wecoma faults, respectively. These rates were similar to, but somewhat higher than, the estimates from retrodeforming the fault. The higher late Pleistocene slip rate is expected, since the point at which the growth strata were measured, originally located at the fault tip, is now 20 km landward of the tip. Since fault slip rates decrease from the center of a fault toward its tip [*Bilham and Bodin*, 1992; *Scholz et al.*, 1993], the retrodeformation method using the entire movement history includes low slip rates from the fault's early history and should yield a lower average rate. The slip rate may also have varied in time over the life of the fault.

Cascadia Transverse Strike-Slip Faults

North Nitinat Fault

Two prominent Washington margin faults, the North Nitinat fault (NNF) and South Nitinat fault (SNF), were initially recognized by one of us (L.D. Kulm) in a 1971 air gun seismic survey on the southern flank of the Nitinat submarine fan (Figure 2). We surveyed the NNF in 1993 using SeaMARC 1A with both 2-km and 5-km swaths and coincident Hydrosweep swath bathymetry. The 5-km swath survey shows that the fault intersects the deformation front at 47°24'N, strikes 282°, and extends 20 km seaward of the deformation front into the Juan de Fuca plate. The NNF intersects and crosses the deformation front at a large slump on the landward vergent frontal-thrust anticline. The NNF cuts and offsets slump debris within the arcuate slump, as well as the slump scarp and the crest of the marginal ridge, 150 m left laterally (Figure 5). At the deformation front the fault offsets landward vergent protothrusts by 300-400 m. Figure 5 shows that these structures and the frontal thrust anticline bend 10-15° to the left where they intersect the NNF. A mud volcano straddles the fault near a right (restraining) bend 9 km seaward of the deformation front (Figure 6). The 2 km swath revealed a submarine channel parallel to the base of the continental slope on the abyssal plain. This channel is cut and offset 150 m left-laterally by the NNF (Figures 5 and 6). The offset channel wall has subsequently slumped (Figure 6), but the left separation is still apparent using the wider swath in Figure 5 to map the channel wall. We estimate the age of the offset channel wall to be 16-20 ka, spanning the last Pleistocene lowstand at 18 ka, when turbidite activity and channel downcutting were at a maximum [*Nelson*, 1968; *Griggs and Kulm*, 1973]. This timing is consistent with activity in other submarine channels on the Cascadia margin, although minor channel cutting continued into the Holocene [*Nelson*, 1968]. The Holocene-late Pleistocene slip rate of this fault, based on the observed offset and inferred channel age, is 8.3 ± 1.0 mm/yr, the error range reflecting uncertainty in the timing of the channel cutting episode. Further evidence of the left-lateral motion on this fault is the presence of a mud volcano at a restraining bend in the fault (Figure 6). We infer that the mud volcano results from elevated pore fluid pressures due to the transpressional fault geometry, resulting in the extrusion of deeply buried abyssal plain sediments.

Restoration of fault motion on the abyssal plain using three seismic profiles (University of Washington (UW) cruise TT-063, 1971) yielded a net left-lateral slip of 2.2 ± 0.3 km for the NNF. The inferred age of the oldest growth strata adjacent to the fault is 400 ± 50 ka, which we take as the time of initial fault motion on the abyssal plain near the deformation front. We assume that horizontal and vertical motion began concurrently and were continuous over the life of the fault. From the calculated net slip and age for the fault

Figure 5. (top) SeaMARC 1A sidescan sonar image of the intersection of the North Nitinat fault and the plate boundary off central Washington. Light areas are high backscatter. Fault offsets the landward-vergent thrust ridge, slump debris, slump headwall scarps, and an abyssal plain channel. The fault is not offset laterally at the plate boundary thrust. Swath width is 5 km. (bottom) Interpretation of the sidescan image. A local 20° bend in the strike of accretionary wedge anticlines occurs across the fault, which widens and branches into multiple traces at the deformation front. Offset of abyssal plain channel is shown in detail in Figure 6. Extensive slumping of the backlimb of the landward vergent frontal anticline of the accretionary wedge may be triggered by strike-slip faulting. Two episodes of slumping are indicated by the glide paths of the younger slump blocks which have overridden earlier slump debris. Some interpretation details are based on 3-D stereo visualization of the imagery and coregistered swath bathymetry.

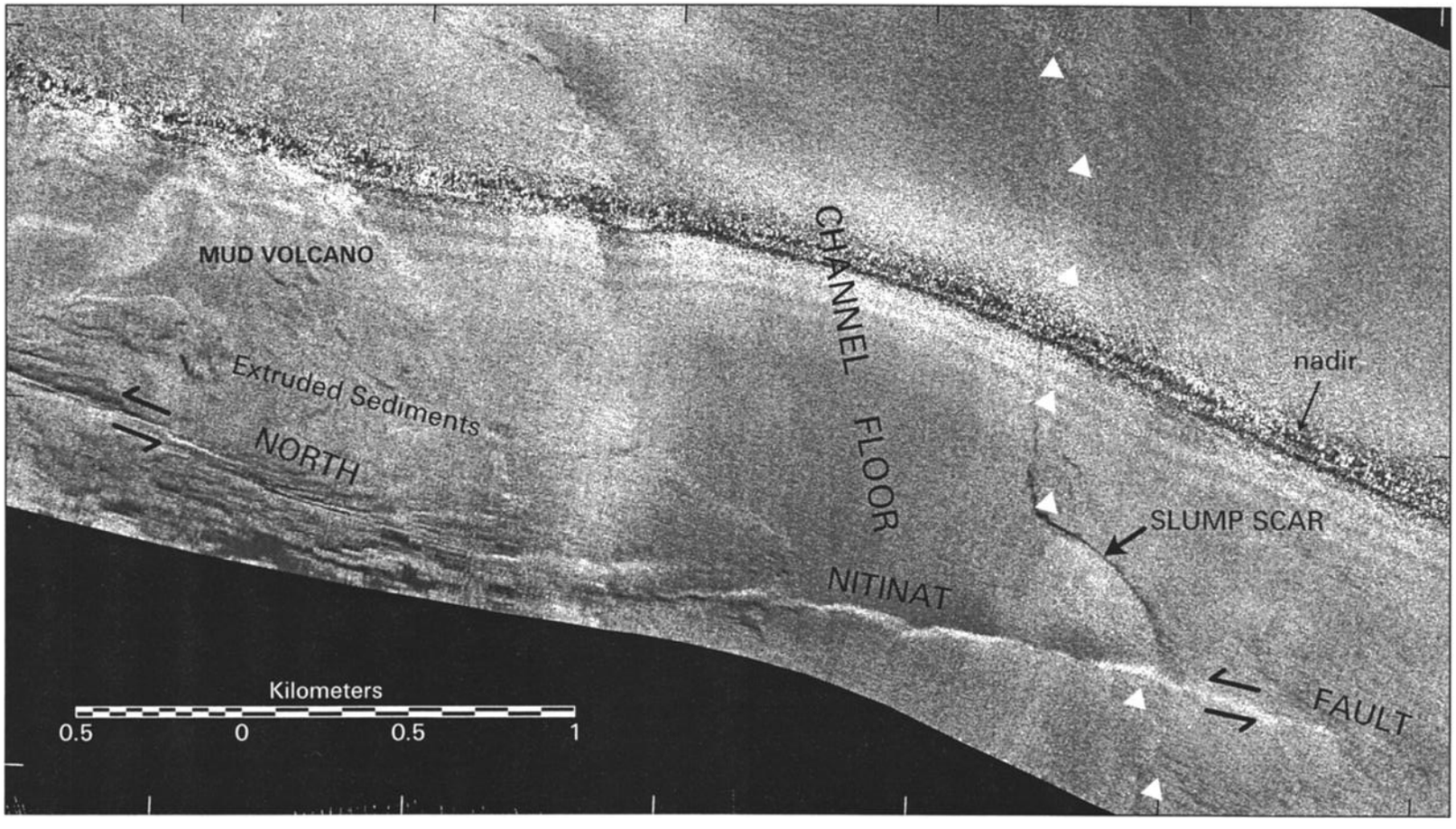

Figure 6. SeaMARC 1A 2-km sonar swath showing an abyssal plain channel offset by the North Nitinat fault. See box in Figure 5 for location. Interpreted original channel wall location, shown by white pointers, was mapped using bathymetry and the 5-km swath south of the coverage of this image (see Figure 5). By projecting the northern channel wall to the fault, we estimate the left offset of the channel wall is approximately 150 m. We interpret the sequence of events from crosscutting relationships as follows: (1) Channel cutting and (2) subsequent offset by the fault, (3) extrusion of sediments from the mud volcano along the fault at left, (4) extruded sediments partially filling the channel and force the flow to the east, and (5) eastward redirected channel flow which triggers slumping of the eastern channel wall, which is not yet offset by the fault.

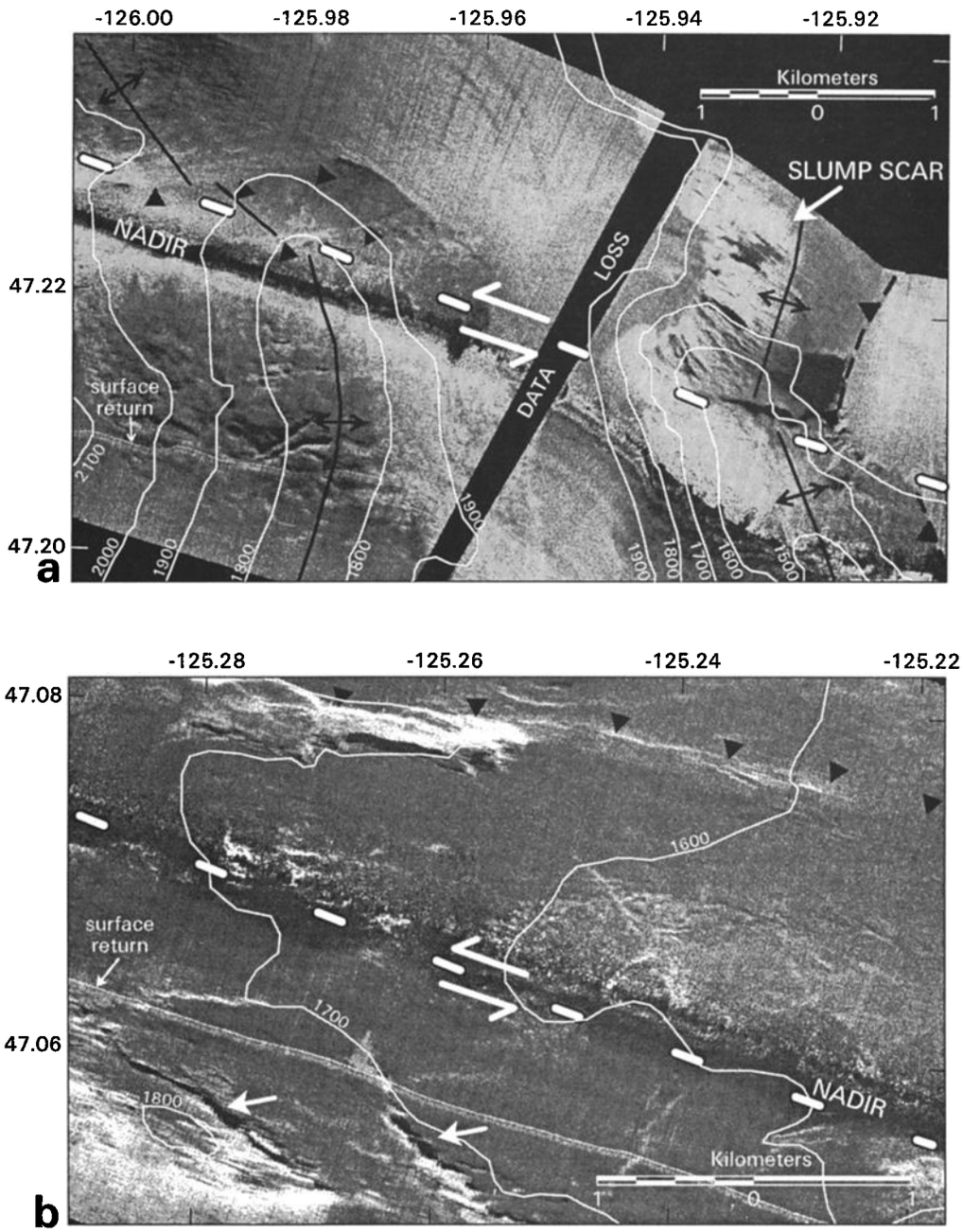

Figure 7. Two SeaMARC 1A 5-km swaths along the North Nitinat fault showing the variable deformation styles along this structure. (a) The third and fourth thrust ridges landward of the deformation front. The western ridge bends sharply left and is offset by individual E-W left-lateral faults. The eastern ridge is also offset along a larger scarp subparallel to the main trend of the NNF, shown by white dashes. (b) The eastern fault tip, showing en echelon fractures at lower left, and a northern trace that we interpret as controlling a headward eroding channel. Overall trend of fault zone is shown by white dashes.

we calculate a slip rate of 5.5 ± 2 mm/yr for the North Nitinat fault. Air gun records from the University of Washington survey did not penetrate to oceanic basement; thus we do not know if the NNF or SNF offset the basaltic oceanic crust.

We traced the NNF southeastward across the continental slope with sidescan sonar using a 5-km swath. Evidence of faulting was observed over a total length of 115 km from the western tip of the NNF to the upper continental slope. The expression of the NNF in the fold-thrust belt of the continental slope was variable. We observed accretionary wedge folds across the lower and middle continental slope that were offset left-laterally, as well as sharply bent, and in several cases offset left-laterally by possible R shears (black arrows in Figure 7a). Subdued linear traces were observed in the intervening synclinal basins. We also observed regions of multiple parallel scarps, en echelon fault strands (Figure 7b), and sigmoidal bends in accretionary wedge thrust anticlines. Determination of net slip on the continental slope

portion of the fault is problematic, as we know of no datable piercing points. Based on the observation that net slip reaches a maximum at a fault's center, we infer that the maximum horizontal slip is larger than the 2.2-km slip observed near the seaward fault tip. The NNF is best expressed in the accretionary wedge thrust ridges and is subdued or absent in the intervening basins. This morphology is also characteristic of the South Nitinat, Willapa Canyon, Wecoma, and Alvin Canyon faults and, to a lesser extent, the Daisy Bank fault. However, the strike-slip faults in southern Oregon are well imaged even in the synclinal basins. We infer that the principal reason for this difference in surficial expression is probably related to a different origin for the southern Oregon faults, discussed in a subsequent section. Second, the low vertical separation across the faults results in little expression of faulting in the broad flat-bottomed basins in northern Oregon and Washington as compared with the steep continental slope of southern Oregon. We speculate that the latitudinal difference in surface expression may also be due to the relatively high sedimentation rates in northern Oregon and Washington as compared with southern Oregon [e.g., *Sternberg*, 1986; *Barnard*, 1978], which would tend to bury or subdue fault traces in the synclinal basins. The greater sediment supply is suggested by the greater thickness of abyssal plain sediment cover due to the Astoria, Nitinat and Willapa submarine fans: 2.5-2.8 s two-way travel time off northern Oregon and central Washington, 2.0 s off southern Oregon.

South Nitinat Fault

The South Nitinat fault (SNF, Figure 2) intersects the deformation front at 47°05.3'N, 19 km south of the North Nitinat fault. The SNF strikes 283°, intersecting the base of slope at a 7.7-km left step in the deformation front, and extends 19 km seaward of the deformation front on the abyssal plain. The base of slope channel offset by the North Nitinat fault also crosses the trace of the SNF adjacent to the accretionary wedge, where the seaward flank of the first thrust ridge forms its eastern bank. The channel bends sharply left as it crosses the fault, suggestive of left-lateral offset, but the channel bathymetry is so subdued that offsetting relationships could not be clearly distinguished in the sidescan data. In a N-S seismic profile (UW TT-063, line 32) the SNF appears virtually identical to the NNF, with a down-to-the-south vertical separation and thickened growth strata on the downthrown block. Eastward thickening prefaulting abyssal plain units thin abruptly from north to south across the fault, indicating left-lateral slip on the SNF. By restoring fault motion, we obtain a net slip for the SNF of 2.0 ± 0.8 km. The restoration reflects greater uncertainty than the NNF restoration due to the somewhat poorer seismic record for the SNF. The depth in the Nitinat fan section at which growth strata appear on the downthrown side of the fault is 302 m; thus, using the Nitinat Fan sedimentation rate of 100 cm/1000 years, the age of the fault is ~ 300 ± 40 ka. From the age and net left-lateral separation we calculate a slip rate of 6.7 ± 3 mm/yr for the South Nitinat fault. We obtained sidescan and Hydrosweep bathymetric data for the seaward 40 km of the fault and attempted, unsuccessfully, to survey the landward part of the fault based on evidence from GLORIA regional sidescan data. GLORIA sidescan imagery suggests that this fault may extend 70 km farther landward.

We have mapped two major active reverse faults on the SW Washington shelf that appear to control the location of the Willapa Basin depocenter (Figure 2) [*Cranswick and Piper*, 1992] and Willapa Bay onshore (L. McNeill et al., Listric normal faulting of the northern Oregon and Washington continental margin, Cascadia subduction zone, submitted to *Journal of Geophysical Research*, 1996). Older structures bend sharply seaward just west of the mapped northern fault (Figure 2). We investigated the northern of these E-W to WNW trending structures with the AMS 150 sidescan system in 1994, suspecting that this structure might be related to the SNF. We observed linear WNW trending backscatter patterns in the sediment but found no surface faulting in the thick Holocene sediments.

Willapa Canyon Fault

The Willapa Canyon fault (WCF) intersects the deformation front at 46°18'N, 8 km south of the outlet of Willapa submarine canyon onto the abyssal plain (Figure 2). This fault cuts the accretionary wedge but does not extend into the abyssal plain as a detectable surface rupture. The seaward projection of the WCF is crossed 4.7 km west of the deformation front by University of Washington reflection line TT 79-1, which shows no disruption of the abyssal plain section, confirming the lack of lower plate involvement west of the plate boundary. On the accretionary wedge, the Willapa Canyon fault is poorly expressed over much of its length but is well expressed near its center, on the mid continental slope, where it offsets left-laterally a northwest trending channel by approximately 900 m. The overall strike of the fault is 280°. No age information is available for the channel; thus we are unable to determine the age or slip rate for the WCF.

Wecoma Fault

We surveyed the entire length of the Wecoma fault using SeaMARC 1A with a 5-km swath width. We investigated the continental slope and outer shelf sections of the fault, as well as the abyssal plain portion from a different illumination angle than the 1989 survey. The new data support earlier interpretations of the continuity of the Wecoma fault as an active structure across the slope [*Goldfinger et al.*, 1992b; 1996a], and we were able to trace this fault to its apparent eastern tip over a total length of 95 km (Figure 2). The Wecoma, Daisy Bank, and Alvin Canyon faults each offset the abyssal plain sedimentary section and the underlying basaltic oceanic crust (Figure 3) [*Goldfinger et al.*, 1992b, 1996a; *Appelgate et al.*, 1992; *MacKay*, 1995]. Near the deformation front, all three fault zones have two main strands dipping steeply toward each other that define popup structures (Figure 3d). The Wecoma fault steps to the right on the abyssal plain, forming a restraining step. A doubly plunging anticline between the two fault strands appears to be caused by this restraining step (left end of Figure 8). This upwarp is cored by oceanic crust, based on the reflection data and modeling of a magnetic profile over the upwarp [*Appelgate et al.*, 1992; *Goldfinger et al.*, 1992b, 1996a].

Goldfinger et al. [1992b, 1996a] estimate the age of the Wecoma fault to be 650 ± 50 ka and the net left-lateral slip to be 5.5 ± 0.8 km. From the age and net left-lateral separation, they calculate a slip rate of 8.5 ± 2 mm/yr for the Wecoma fault. Offset of a dated channel 5 km west of the deformation

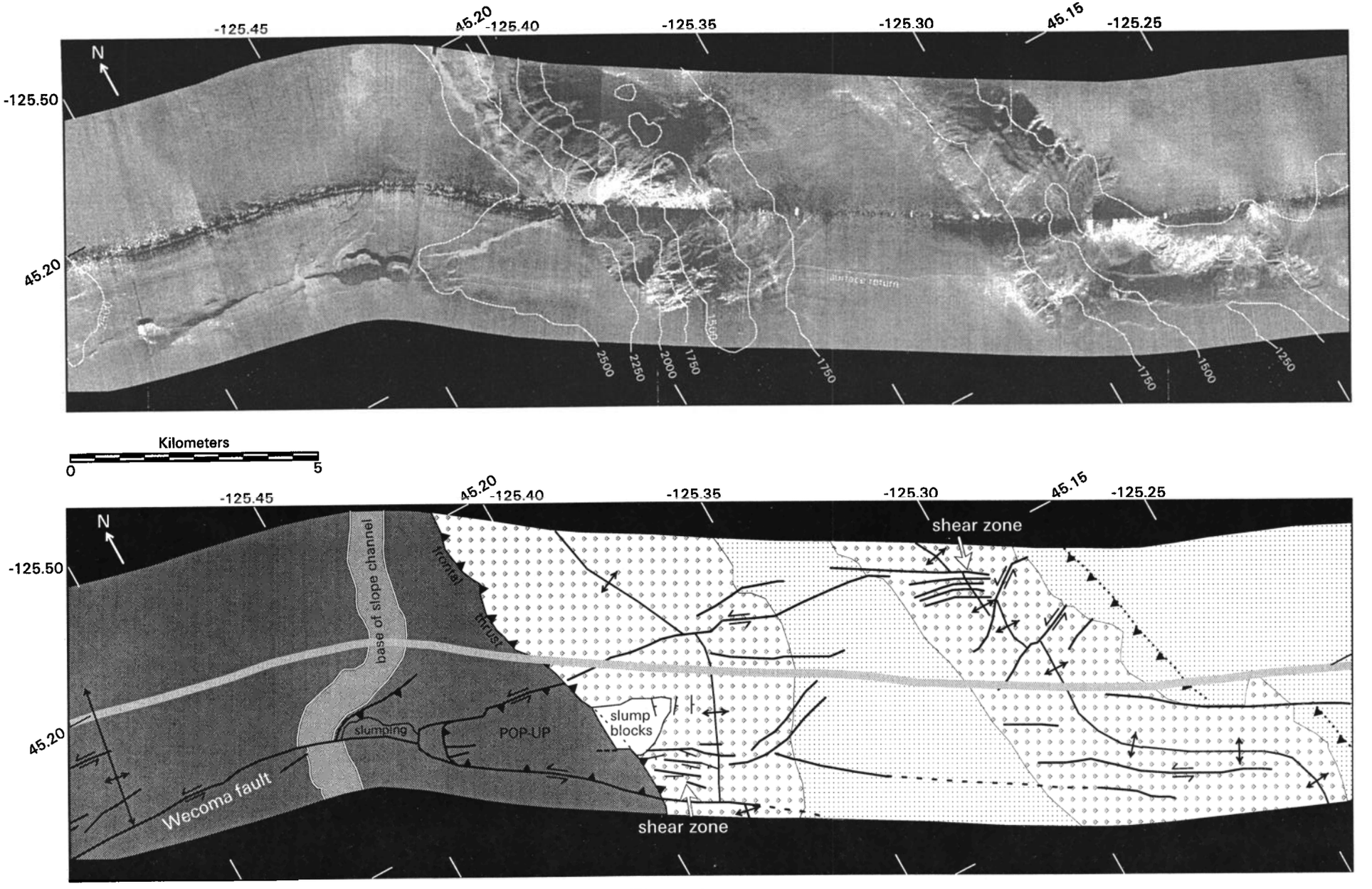
-125.45
45.20
-125.40
-125.35
-125.30
45.15
-125.25
N
-125.50
45.20
surface return
2500
2250
2000
1750
1750
1750
1500
1250
Kilometers
0
5
-125.45
45.20
-125.40
-125.35
-125.30
45.15
-125.25
N
-125.50
45.20
shear zone
base of slope channel
frontal thrust
slumping
POP-UP
slump blocks
Wecoma fault
shear zone

Figure 8.

front allowed independent calculation of a slip rate of 8.5 ± 4 mm/yr for the Wecoma fault [*Appelgate et al.*, 1992; *Goldfinger et al.*, 1992b, 1996a]. Figure 8 shows a SeaMARC 1A 5-km sidescan swath over the Wecoma fault on the abyssal plain and lower continental slope. The surficial fault trace splits into two faults defining a popup structure just seaward of the deformation front. Both strands extend across the frontal two thrust anticlines, beyond which the northern strand may die out. Between the two strands, the frontal thrust vergence reverses to seaward from the regional landward vergence direction. Multichannel reflection data do not clearly image these faults in the complex accretionary wedge. Nevertheless, the sonar imagery shows shear zones exposed at the crests of these two ridges, as well as bends and offsets of the anticlinal axes (Figure 8). The second thrust ridge is offset by a series of NE-SW trending left-lateral en echelon faults between the two strands of the Wecoma fault, and the second anticlinal ridge bends sharply to the left as it crosses the fault (Figure 8). The third ridge terminates at the fault. Extensive methane-rich fluid venting was observed along the southern strand on the frontal thrust anticline [*Tobin et al.*, 1993]. Bedding attitudes taken from the submersible *Alvin* show that dips are rotated into parallelism with the Wecoma fault within this same area, which is on the seaward limb of the seaward vergent frontal thrust (Figure 8) [*Tobin et al.*, 1993].

The Wecoma fault, like the Daisy Bank, Alvin Canyon, and the three Washington faults, is subdued in surface expression in the lower slope basins but prominent on the anticlinal ridges and on the middle and upper continental slope. SeaMARC 1A imagery shows that the Wecoma fault consists of multiple surficial fault traces in a zone of deformation that increases in width landward. Young folds on the lower slope are commonly deflected or offset to the left at the fault and show marked increased elevation near the fault. On the middle to upper slope, several prominent folds bend sharply to an orientation parallel to the Wecoma fault from the regional NNW fold trend. These and several other folds parallel the Wecoma fault for a distance of 15 km (Figure 9). The area shown in Figure 9 appears to be either a large right (compressional) step or complex deformation between two strands of the Wecoma fault. The right side of Figure 9 is near the eastern tip of the Wecoma fault, and the sonar image shows the fault bending toward the northeast in a probable horse-tail splay. Fold axes in the southeast and northwest parts of Figure 9 are offset left-laterally. Additionally, left-stepping en echelon folds along the fault indicate the overall shear sense of the Wecoma fault is sinistral [e.g., *Wilcox et al.*, 1973; *Harding and Lowell*, 1979; *Sylvester*, 1988], in agreement with the observed separations. The entire Wecoma fault zone lies in a broad parallel swale visible in SeaBeam bathymetry. A proprietary seismic reflection profile shows the fault and associated positive flower structure, which abruptly truncate an adjacent syncline (Figure 10). OSU sparker line SP-54 shows a similar truncation by the high-angle fault, and a possible second vertical strand 2.2 km to the north (Figure 11; 8 km east on the E-W profile).

The surface trace of the Wecoma fault on the sidescan records terminated at 44°54.8'N, 124°35.93'W. This area of the outermost shelf was covered with ripples and sand waves in unconsolidated sand, confirmed by two *Delta* submersible dives in 1992 and 1993. The unconsolidated and mobile sediment made locating the eastern fault tip problematic. The Wecoma fault appears to terminate near the inferred western limit of the Siletzia terrane shown in Figure 2. The terrane boundary is inferred on the basis of the strong magnetic signature of the underlying Siletz block and by velocity analysis of a wide-angle reflection profile just to the south of the Wecoma fault [*Tréhu et al.*, 1995]. SeaBeam bathymetry data and numerous reflection profiles show this boundary to mark a profound change in structural style across the forearc. The rapidly deforming fold-thrust belt of the active accretionary wedge gives way to gentle open folds landward of the Siletzia boundary. SeaBeam data reveal a series of short NW trending en echelon folds just seaward of the boundary, suggestive of right-lateral shear. *Snavely* [1987] infers that the dextral Fulmar fault controls the location of the seaward edge of the Siletzia block, and *Tréhu et al.* [1995] suggest that a fault observed overlying the terrane boundary may be the active Fulmar fault. Our data also show a fault near the western edge of Siletzia (eastern fault in Figure 11), although the SeaMARC 1A data show this fault to be NW trending. Thus we are uncertain whether this structure is related to the Siletzia boundary or is the eastern tip of the Wecoma fault.

Daisy Bank Fault

We surveyed the entire length of the Daisy Bank fault (DBF; fault B of *Goldfinger et al.* [1992b] using the SeaMARC 1A system on the abyssal plain and slope and the AMS 150 system on the upper slope and shelf. Figure 3 shows the Daisy Bank fault immediately west of the deformation front. The DBF extends 21 km seaward of the deformation front onto the abyssal plain where surface and subsurface expression die out. The main fault trace intersects a 150-m-high ridge along the boundary between the landward vergent thrust ramp and the fault. MCS lines 37 (Figure 3b) and 19 (not shown) show this ridge to be a southwest vergent thrust ridge bounded by the DBF on its southern flank. The main strand of the DBF steps to the right at the western end of this anticlinal ridge and continues to the northwest. We interpret the fold as a pressure ridge developed between the two overlapping fault strands similar to the fold along the Wecoma fault [*Goldfinger et al.*, 1992a; 1996b]. Basement reflectors show two offsets, one

Figure 8. (top) SeaMARC 1A sidescan image of the Wecoma fault zone on the abyssal plain and crossing the frontal and second accretionary wedge anticlines. (bottom) Interpretation. The single-stranded fault bifurcates, defining a popup structure just seaward of the frontal thrust. Both fault strands cross both ridges and the intervening basin, although they are faint in the basin. The second ridge is offset by a series of possible synthetic left-lateral faults. The second ridge bends sharply at the southern fault strand, forming a steep, highly reflective scarp at right. The third ridge (not shown) terminates at the southern fault strand. Strike and dip symbols in and north of western shear zone from Alvin observations [*Tobin et al.*, 1993].

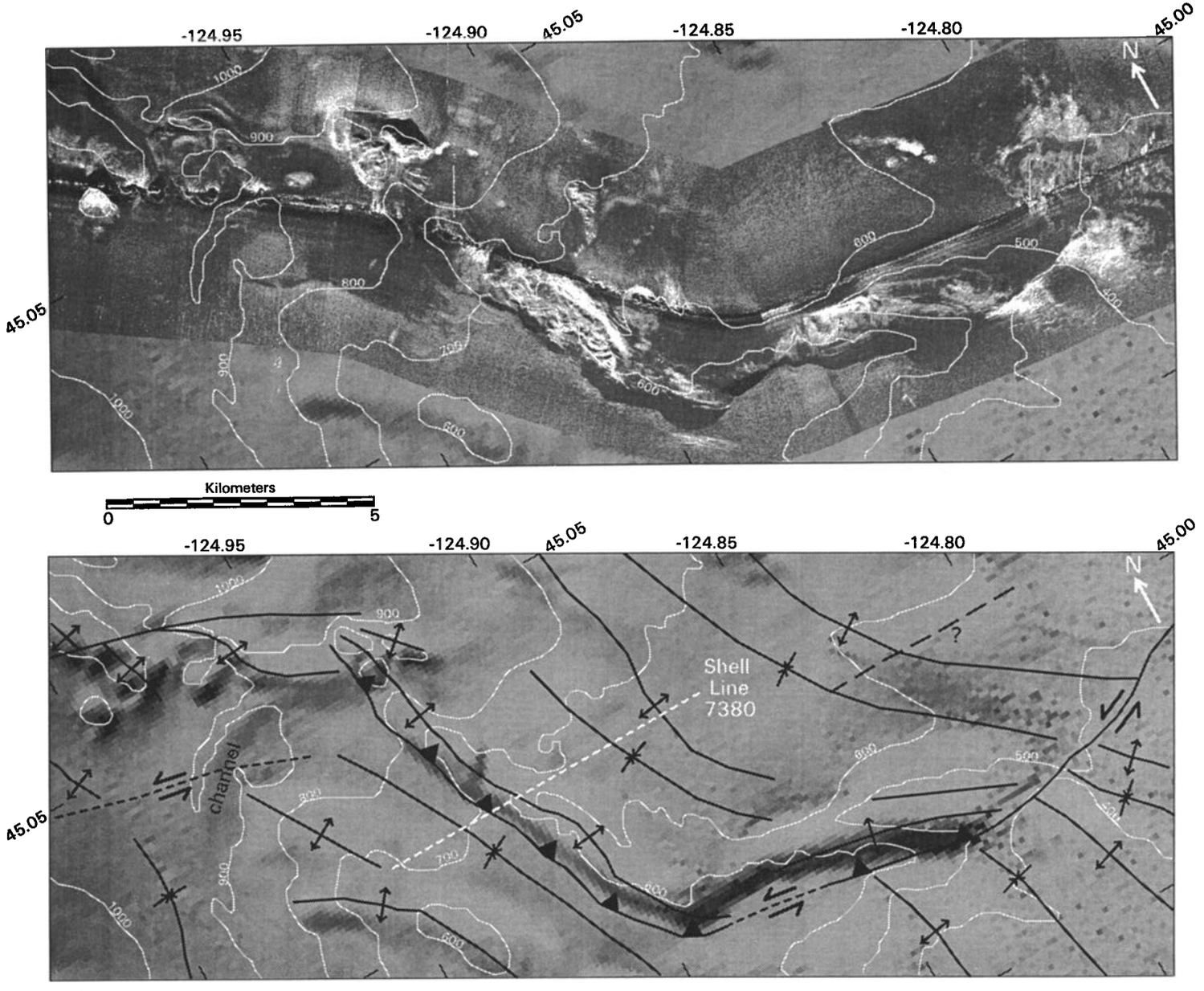

Figure 9. (top) SeaMARC 1A sidescan image of the Wecoma fault zone at a complex right (transpressional) step on the upper continental slope off central Oregon, overlain on SeaBeam bathymetry. (bottom) Interpretation. A series of NW trending folds are offset or bent left-laterally in this area. Fold axis offsets mapped from reflection data, sidescan, and bathymetry are revised from *Goldfinger et al.* [1992a]. Location of Shell seismic profile in Figure 10 is shown in white dashes. Light tones are high backscatter, and bathymetry is illuminated from the north. Swath width is 5 km.

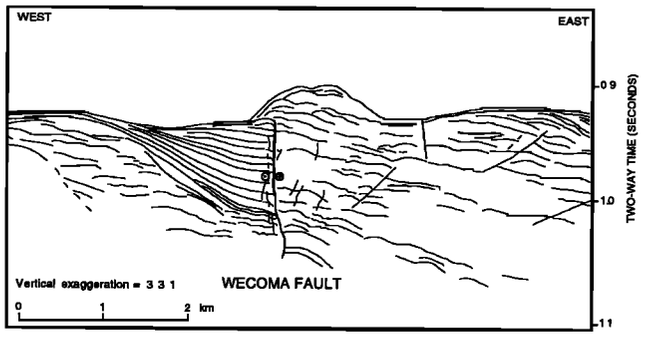

Figure 10. Line drawing of Shell Oil Company sparker line 7380 on the middle continental slope off central Oregon. Location is shown on Figure 9. The Wecoma fault truncates a NNW trending syncline. We interpret this structure as a transpressional oblique-slipping fault segment that is accommodating a regional right step of the Wecoma fault zone.

up-to-the-north and one up-to-the-south, that define a "popup" of the basement across the DBF on MCS line 37 (Figure 3b).

The intersection of the DBF and the accretionary wedge marks an abrupt transition in structural domains between seaward vergent thrusts (seaward directed thrusting) southward to 42°10'N and landward vergent thrusts (landward directed thrusting) northward to Barkley Canyon at 48°12'N [*MacKay et al.*, 1992; *MacKay*, 1995; *Goldfinger et al.*, 1996b]. *Goldfinger et al.* [1996b] interpret a progressive vergence reversal from south to north along a 15-km distance along the margin south of the DBF. The 1989 MCS data suggest progressive undercutting of an originally landward vergent ridge by a younger seaward vergent thrust. The vergence reversal that appears to be localized by the DBF has apparently progressed from south to north, suggesting passage of the DBF beneath the margin.

We determined the geometry of pre-faulting eastward thickening abyssal plain sediment wedges using MCS lines 05-08 for the Daisy Bank fault. Retrodeformation of the abyssal plain section yielded a net left-lateral separation of 2.2 ± 0.5 km. The depth to the oldest growth strata is 360 m, determined from MCS line 37. From the sedimentation rate of 94 cm/1000 years, we obtain an age of 380 ± 50 ka for the DBF. The age and net slip values yield a slip rate of 5.7 ± 2 mm/yr for the Daisy Bank fault.

Using SeaMARC 1A sidescan imagery, we traced the Daisy Bank fault zone across the lower continental slope (Figure 12). As with the other northern Oregon and Washington faults, the fault morphology is subdued on the lower slope relative to the upper slope or abyssal plain. The DBF is characterized by discontinuous fault traces that disrupt thrust anticlines and, to a lesser degree, the intervening basins. One 3 to 4-km long strand terminates at the foot of a thrust ridge, producing gullies and a prominent slump scarp. Farther seaward, several splays of the DBF truncate the frontal thrust anticline of the accretionary wedge. Reversals of vertical separation occur along this ridge, with several tens of meters of relief evident along the main splay. The DBF crosses the boundary between the Juan de Fuca and North American plates in a 1 km-wide fault zone that appears to have localized slumping of the seaward limb of the frontal thrust.

Daisy Bank, on the upper continental slope, is one of several uplifted Neogene structural highs off Oregon [*Kulm and Fowler*, 1974]. The DBF bounds the southern flank of Daisy Bank; a second less prominent strand of the fault bounds the northern flank. SeaMARC 1A sidescan imagery and multichannel (MCS) and single channel (SCS) seismic reflection data show that the Daisy Bank fault is a wide structural zone, within which Daisy Bank is uplifted as a horst between two strands of the main fault. The main fault zone is 5-6 km wide northwest of Daisy Bank, widening around the oblong bank, then narrowing to a single strand to the southeast. The traces of the fault strands are straight, implying a near vertical fault. Probable drag folds of exposed strata, with a left-lateral sense of motion, are visible in sidescan imagery southeast of the bank (Figure 12). Mapping from seismic reflection profiles indicates left-lateral offsets of NNW trending accretionary wedge fold axes at Daisy Bank (Figure 12). Scarp heights measured from the *Delta* submersible range from tens of centimeters to 47 m. The net uplift of the southern flank of Daisy Bank by both folding and faulting is about 130 m. From *Delta*, we traced one of the Daisy Bank scarps into an area of low relief and mud deposition. We observed a fresh scarp striking 290° across the unconsolidated Holocene mud, which is visible in the AMS 150-kHz sidescan images (Figure 12). Stratigraphic relationships indicate post 12-ka motion on this segment of the Daisy Bank fault [*Goldfinger et al.*, 1996b].

The mapped eastern tip of the Daisy Bank fault overlies the Siletzia terrane boundary as does the Wecoma fault, thus we infer that the Daisy Bank fault probably terminates against

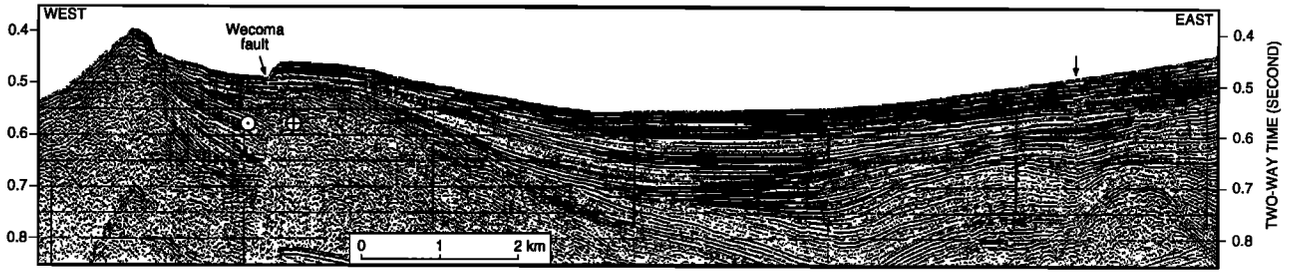

Figure 11. OSU single-channel sparker profile SP-54. A prominent strand of the Wecoma fault juxtaposes an anticline and syncline at left. The second subvertical fault at right is probably also a strike-slip structure and may either be the dying northern strand of the Wecoma fault or the Fulmar fault. See Figure 16 for location and text for discussion.

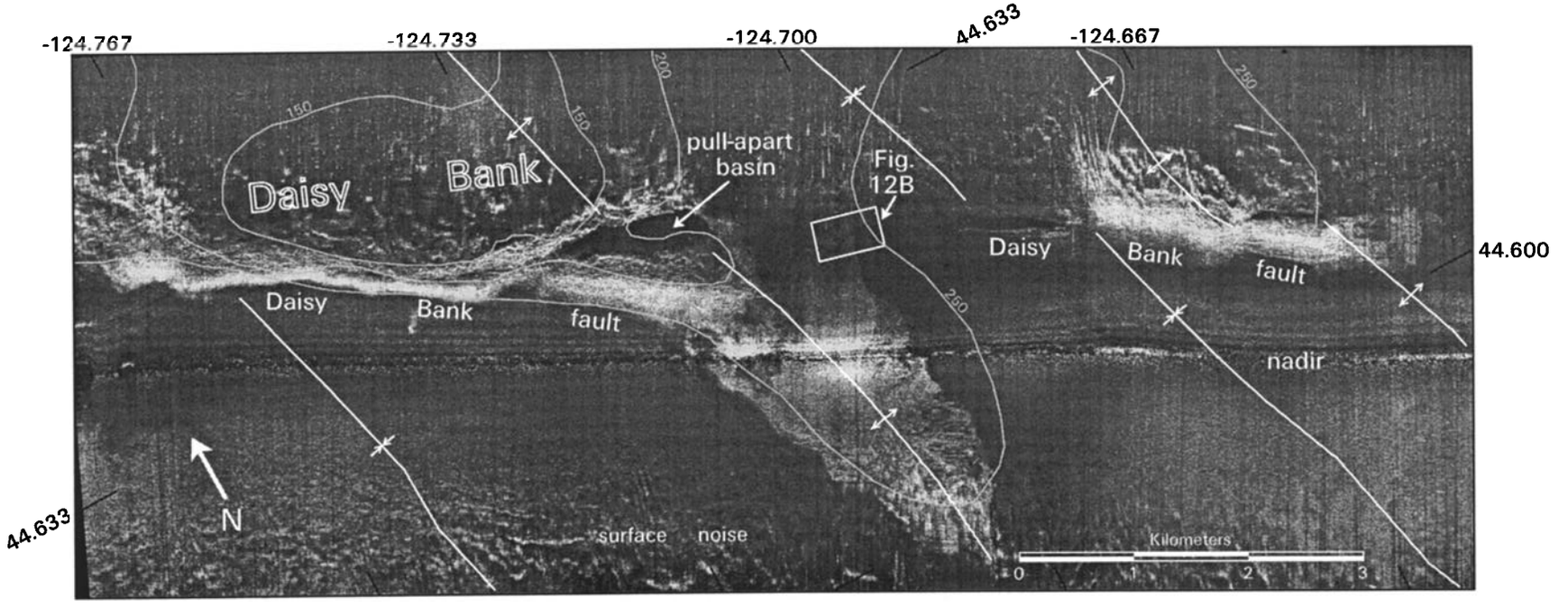

Figure 12a. Sidescan sonar image of the Daisy Bank fault (DBF), upper continental slope of central Oregon. Light tones are high backscatter. SeaMARC 1A image (5-km swath) shows Daisy Bank in upper left. Total relief on main scarp is 130 m at Daisy Bank, and 47 m at eastern scarp. Left-lateral offset of fold axes (mapped from reflection profiles, sidescan, and bathymetry data) is shown. A small pull-apart basin formed across a left stepover of the main scarp. Left-lateral drag folding of bedding shown adjacent to the eastern scarp.

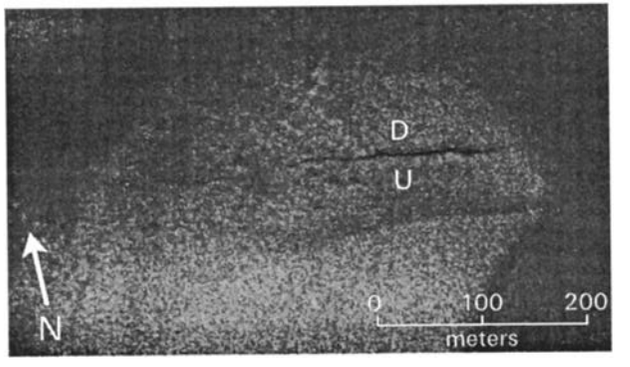

Figure 12b. High-resolution AMS 150-kHz sidescan image showing offset of unconsolidated Holocene sediments [*Goldfinger et al.*, 1996b].

the Siletzia terrane, giving a mapped length of 94 km. Further details of the Daisy Bank fault are given by *Goldfinger et al.* [1996b].

Alvin Canyon Fault

The Alvin Canyon fault (ACF), named for its proximity to a series of *Alvin* dive sites, is similar in structural style to the Daisy Bank fault. Its structural details are not as well known, since it has not been surveyed with sidescan sonar on the continental slope. The fault was mapped from 1989 SeaMARC 1A sidescan data on the abyssal plain and from seismic reflection profiles and SeaBeam swath bathymetric data on the continental slope. The Alvin Canyon fault extends approximately 7 km seaward of the deformation front, based on sidescan data and two reflection profile crossings on the abyssal plain. The intersection of the fault with the deformation front is marked by a 3.7-km left step in the basal thrust and initial ridge of the accretionary wedge. Linear patterns of authigenic carbonates mapped on the lower slope extend landward from the intersection of the ACF and the base of slope, parallel to the fault trace [*Carson et al.*, 1994]. *Carson et al.* [1994] used reprocessed GLORIA sidescan imagery with the topographic effects of reflectivity subtracted from the image to identify zones of carbonate precipitation. The highly reflective carbonate-bearing sediments are the product of fluid venting of methane-rich pore fluids that have been sampled directly by submersible in the immediate area [*Kulm and Suess*, 1990] and are commonly associated with fault zones elsewhere on the slope [*Kulm and Suess*, 1990; *Tobin et al.*, 1993; *Goldfinger et al.*, 1996b].

We retrodeformed prefaulting stratal wedges using MCS lines 01-05 to define the geometry of prefaulting units. We calculate a net 2.2 ± 0.5 km of left-lateral separation for the Alvin Canyon fault. We estimate a sedimentation rate of 79 cm/1000 years for the Astoria fan section at the Alvin Canyon fault. A depth of 310 m for the oldest growth strata was determined from MCS line 37 using the depth in two-way time and the sedimentation rate. Using the sedimentation rate and depth values, we obtain an age of 380 ± 50 ka for the initiation of motion on the fault. These values yield a slip rate of 6.2 ± 2 mm/yr for the Alvin Canyon fault.

Like the Daisy Bank fault, the Alvin Canyon fault widens from a single strand on the abyssal plain to a 6-km-wide fault zone on the upper slope. The Alvin Canyon fault has strong morphological similarities to the better surveyed Wecoma and Daisy Bank faults. An unnamed submarine bank is uplifted as a horst between two strands of the fault, similar to the structural setting of Daisy Bank. Like Daisy Bank, this horst has been truncated by erosion during Pleistocene low sea level stands. On the abyssal plain, Holocene seafloor sediments are offset by the Alvin Canyon fault, suggesting that it is likely to be an active structure on the slope, but this cannot be confirmed without further investigation.

Heceta Bank Structure and Heceta South Fault

The Heceta Bank structure is centered at approximately 43°56'N on the continental slope (Figure 2), strikes 308°, and has a minimum length of 16-20 km (Figure 13). This structure bounds the southeastern flank of Heceta Bank, a complex anticlinorium that has undergone up to 1000 m of post-Miocene uplift [*Kulm and Fowler*, 1974]. The Heceta Bank structure is a striking linear feature that abruptly truncates the uplifted bank. Swath bathymetric data from a NOAA shallow water system (BSSS) revealed that Heceta Bank has at least one submerged Pleistocene lowstand shoreline fringing its western and northwestern flanks (C. Goldfinger, unpublished data, 1993). A smooth wave-cut platform seaward of the former shoreline is clearly visible for a length of 45 km in the bathymetric data, as are former beach berms and probable subaerial drainage features. The submerged shoreline is tilted to the south, deepening from 115 m at the northern end of Heceta Bank to 225 m adjacent to the Heceta Bank structure. A possible continuation of the submerged shoreline and wave-cut platform south of the fault suggests > 200 m of vertical separation across this structure. However, a Klein 50-kHz sonar survey in 1992 failed to identify any offset surficial features from which to characterize the horizontal separation (if any) across this structure. Sidescan data from this survey and subsequent dives with the submersible *Delta* identified areas of tabular carbonate deposition indicative of methane-bearing fluid venting at the top of the scarp, but this evidence was subdued in comparison to other active faults. The scarp itself had a relatively low slope, and no evidence of surface rupture was found in several oblique traverses with *Delta*, nor on the sidescan imagery. An unmigrated multichannel reflection profile (USGS line WO 77-05) shows only weak evidence for faulting and suggests a principally monoclinal structure. The present surface morphology may in part be erosional accentuation of the monocline by wave action during Pleistocene low stands. We conclude that either the Heceta Bank structure is a monocline (presumably overlying a more deeply buried fault) or a strike-slip fault in which lateral motion is not resolved on the reflection profile.

The Heceta South fault lies 15 km west of the Heceta Bank fault and was originally mapped as being the same structure [*Goldfinger et al.*, 1992a]. Subsequent interpretation of SeaMARC 1A sidescan and swath bathymetry data shows that they are two separate structures. The Heceta South fault is 35 km in length and is composed of multiple segments striking 293°-325° (Figure 13). The scarp of the seaward fault segment forms the northern rim of a slump scar on the lower continental slope (Figure 13). This slump, approximately 7.5 km in diameter, involved approximately 14 km^3 of accreted material from the accretionary wedge. Of three known slumps of this magnitude on the Oregon and Washington margins, two occur at the intersection of WNW trending strike-slip faults with the deformation front (North Nitinat fault, Figure 5; Heceta South fault, Figure 13). The Heceta South fault appears to extend several kilometers into the abyssal plain, suggested by the linear truncation of debris from the slump along the projection of the fault, although no seismic reflection data crossing the possible abyssal plain extension of the fault are available to confirm this. Alternatively, the linear trends in the slump debris may have originated along the fault prior to slumping and were then translated onto the plain during the slump event. Sidescan and bathymetric data revealed no piercing points from which to determine horizontal separation for this fault.

Coos Basin Fault

The Coos Basin fault intersects the base of slope at a 1.2-km left step in the deformation front at 44°04'N (Figure 2). We observed no evidence for abyssal plain rupture seaward of the intersection of the fault and the deformation front in

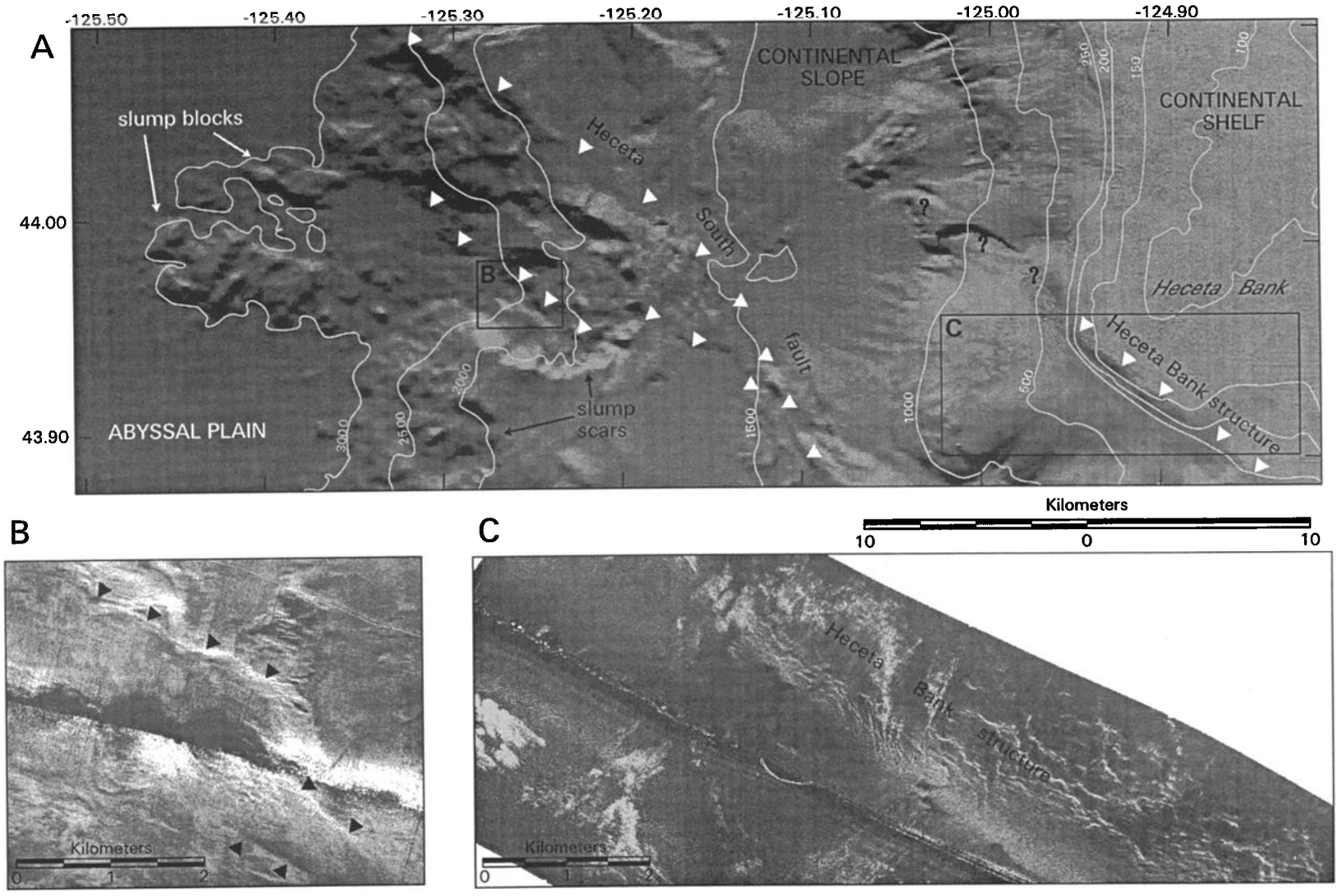

Figure 13. (a) SeaBeam bathymetry and SeaMARC 1A sidescan data showing the Heceta South fault and Heceta Bank structure off central Oregon. The Heceta South fault is a diffuse structure that appears to localize a large slump of the lowermost slope. (b) A SeaMARC 1A image of the fault trace at the foot of the slump headwall scarp. The Heceta Bank structure, at lower right appears to be a monocline but is a striking linear feature subparallel to the other strike-slip faults. (c) A SeaMARC 1A image of the Heceta Bank structure and associated carbonate bearing sediments (white lineations).

sidescan images. Near-surface faulting approximately along the seaward extension of both the Coos Basin fault and Thompson Ridge faults is visible on two-channel seismic reflection records on the abyssal plain [*EEZ-SCAN 84 Scientific Staff*, 1986]. These faults could not be tied to the observed upper plate faults, nor are their strikes known from the single seismic profile. The surficial expression of the Coos Basin fault is an approximately 5-km-wide zone of deformation, the major elements of which are visible in GLORIA sidescan imagery. Two main scarps offset anticlinal ridges on the lower slope left-laterally, and the broad zone is expressed bathymetrically as linear trends striking 288°-293°. Two measured left-lateral offsets of surficial features of 125 and 158 m are visible in a 10-km-wide SeaMARC 1A mosaic collected in 1993. The two well-defined strands of the fault diverge southeastward into a broader structural zone which loses definition about 35 km landward of the base of the continental slope.

Thompson Ridge Fault

The Thompson Ridge fault intersects the base of the continental slope at a 6 km left step in the deformation front at latitude 43°16.5'N (Figure 2), and, like the Coos Basin fault, does not extend into the abyssal plain as a surficial feature based on SeaMARC 1A imagery and SeaBeam data. The Thompson Ridge fault is the best expressed bathymetrically of the nine Cascadia strike-slip faults mapped to date. The main scarp at the deformation front along the left step is 650 m in height, north block up. The fault zone is clearly observed in SeaBeam bathymetry as a pattern of disruption of accretionary wedge thrust ridges, and like many of the other faults, its component strands diverge slightly to the southeast. Figure 14 shows a perspective shaded-relief image of NOAA SeaBeam swath bathymetry data in the Thompson Ridge fault area, gridded to a 100-m point spacing. In map view, a pattern of left steps and sigmoidal bending and offset of crossing folds indicates left-lateral shear. The SeaBeam bathymetry suggests three left stepping anticlinoria (Figure 14), indicating the overall shear sense of the Thompson Ridge fault is sinistral. Other related folds parallel the strike of the fault zone. Crossing thrust ridges step to the left and are elevated at the fault zone, a distinctive morphology also observed at the Wecoma and Daisy Bank faults. This elevation difference, in the case of the Wecoma fault, is the result of a compressional flower structure composed of fault splays with a small reverse component of motion based on seismic reflection records. We infer that much of the bathymetric expression of the strike-slip faults observed on the slope is due to the superimposition of flower structures on the coeval or older thrust ridges. Equipment damage prevented the acquisition of all but a short segment of sidescan data over the Thompson Ridge fault.

Discussion

Basement Involvement

Five of the strike-slip faults (North and South Nitinat, Wecoma, Daisy Bank, and Alvin Canyon faults) cross the plate boundary and are observed in both upper and lower plates (Figure 2). Reflection data for the three Oregon faults suggest that seaward of the deformation front, the entire sedimentary section and the basement are offset by these structures [*Goldfinger et al.*, 1992b; 1996a; *Appelgate et al.*, 1992; *MacKay*, 1995]. These three faults dip steeply to the northeast and bound the southern flanks of asymmetrical basement pop ups (Figure 3d). Magnetic modeling of the Wecoma fault zone indicates that the basement is both offset and significantly upwarped beneath a pressure ridge anticline formed at a right step in the fault trace [*Goldfinger et al.*, 1992b; 1996a; *Appelgate et al.*, 1992]. The basement popups clearly show involvement of the basement in the transverse deformation of the Cascadia forearc, and indicate that these three faults are slightly transpressional. The reflection data for the Washington faults did not reach basement; however, their striking similarity to the Oregon faults suggests similar origins and thus probable basement involvement.

Although the 1989 reflection data clearly resolve basement offset on the three Oregon faults, we are unable to discriminate between throughgoing rupture of oceanic crust or a more superficial detachment of upper crustal blocks such as may have emplaced basaltic blocks in the Franciscan subduction complex in northern California [e.g., *Kimura et al.*, 1996]. However, high pore fluid pressure and very low wedge taper in northern Oregon and Washington, discussed further below, suggest that the lower continental slope is poorly coupled to the subducting plate. The basement offsets observed seaward of the deformation front, therefore, are unlikely to be the result of detachment of basaltic blocks as a direct result of interaction between the accretionary wedge and the slab.

We note a consistent longitudinal pattern of deformation along the faults that extend seaward of the base of slope: strong expression on the abyssal plain, poor expression on the lower slope, and strong expression on the upper slope and outermost shelf. For several reasons, we infer that this pattern is most consistent with faults that originate in the slab and propagate up through the upper plate. Pore fluid pressure in accreted sediments near the plate boundary is known to be high. Negative polarity reflections in décollement zones at the toe of the Oregon slope and a subhorizontal maximum compressive stress suggest highly overpressured dilatant zones at the plate boundary [*Moore et al.*, 1995a]. Fluid pressures in the range of 0.9-0.95 lithostatic are estimated for the Barbados accretionary wedge based on recent logging from drilling results from ODP Leg 156 [*Moore et al.*, 1995b]. During the 1993 SeaMARC 1A survey we observed mud volcanoes on the lower slope and plain off Oregon and Washington, implying lithostatic fluid pressures within the accreted section. The lower slope off northern Oregon and Washington has a very low wedge taper and widely spaced landward vergent folds, further indication of a very weak décollement due to high pore fluid pressure in this region [*Seely*, 1977; *Davis et al.*, 1983; *MacKay*, 1995]. We speculate that the longitudinal pattern of morphologic expression along the transverse faults can be explained by reduced transmission of lower plate fault slip across the overpressured and poorly coupled décollement beneath the lower slope. Rejuvenation of the faults on the upper slope is consistent with progressive dewatering of the wedge, resulting in better interplate coupling as would be expected for the rearward part of the wedge. The landward widening fault zones (Figure 2) are also consistent with fault slip transmitted upward through the eastward thickening accretionary wedge. The slip distribution on the Wecoma fault, determined by

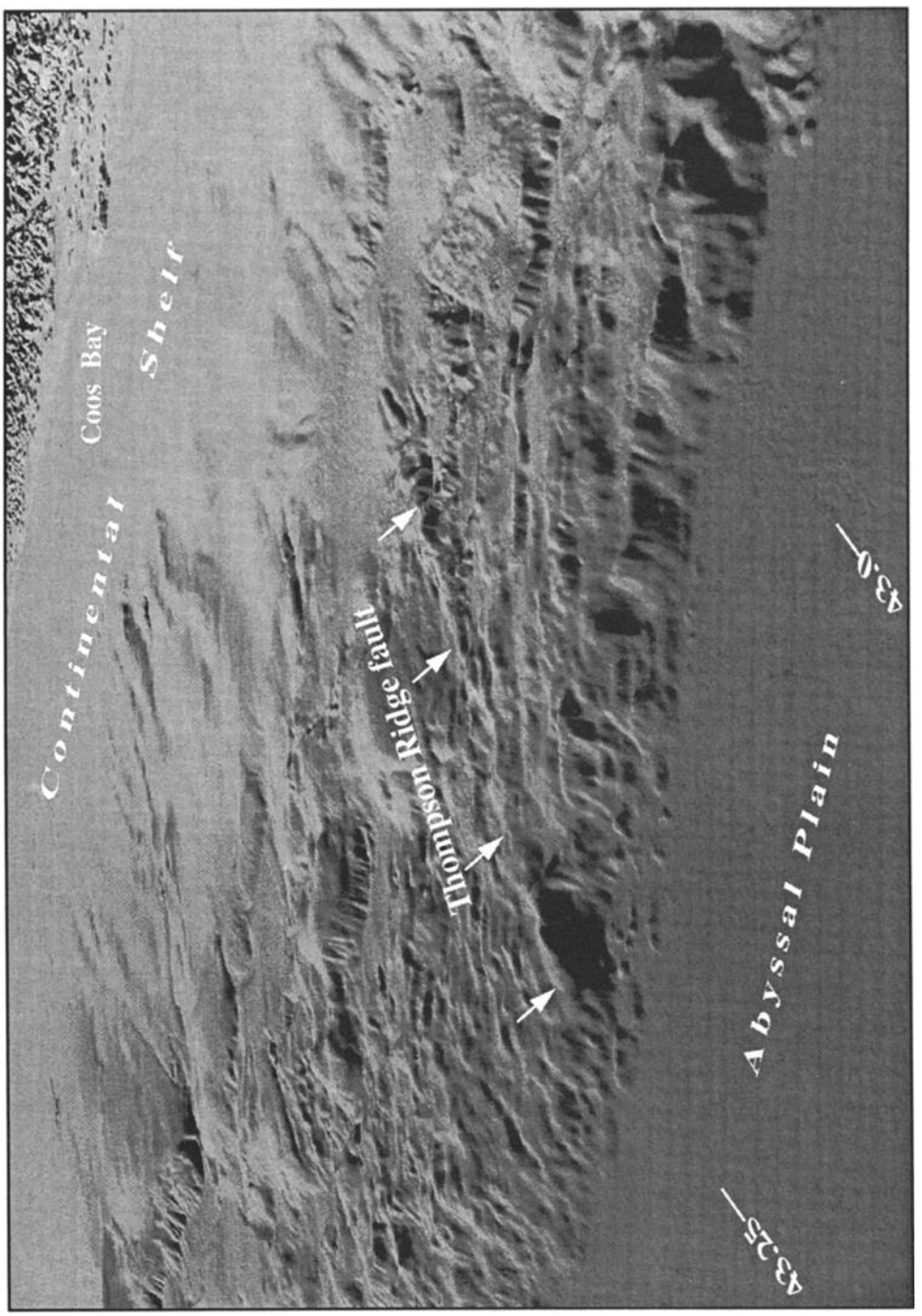

Figure 14. Perspective view of the Thompson Ridge fault, southern Oregon continental slope. Arrows indicate fault and associated folding. Left step in the deformation front visible at western fault tip. Image data is from a 100-m grid of bathymetric and topographic data for western Oregon.

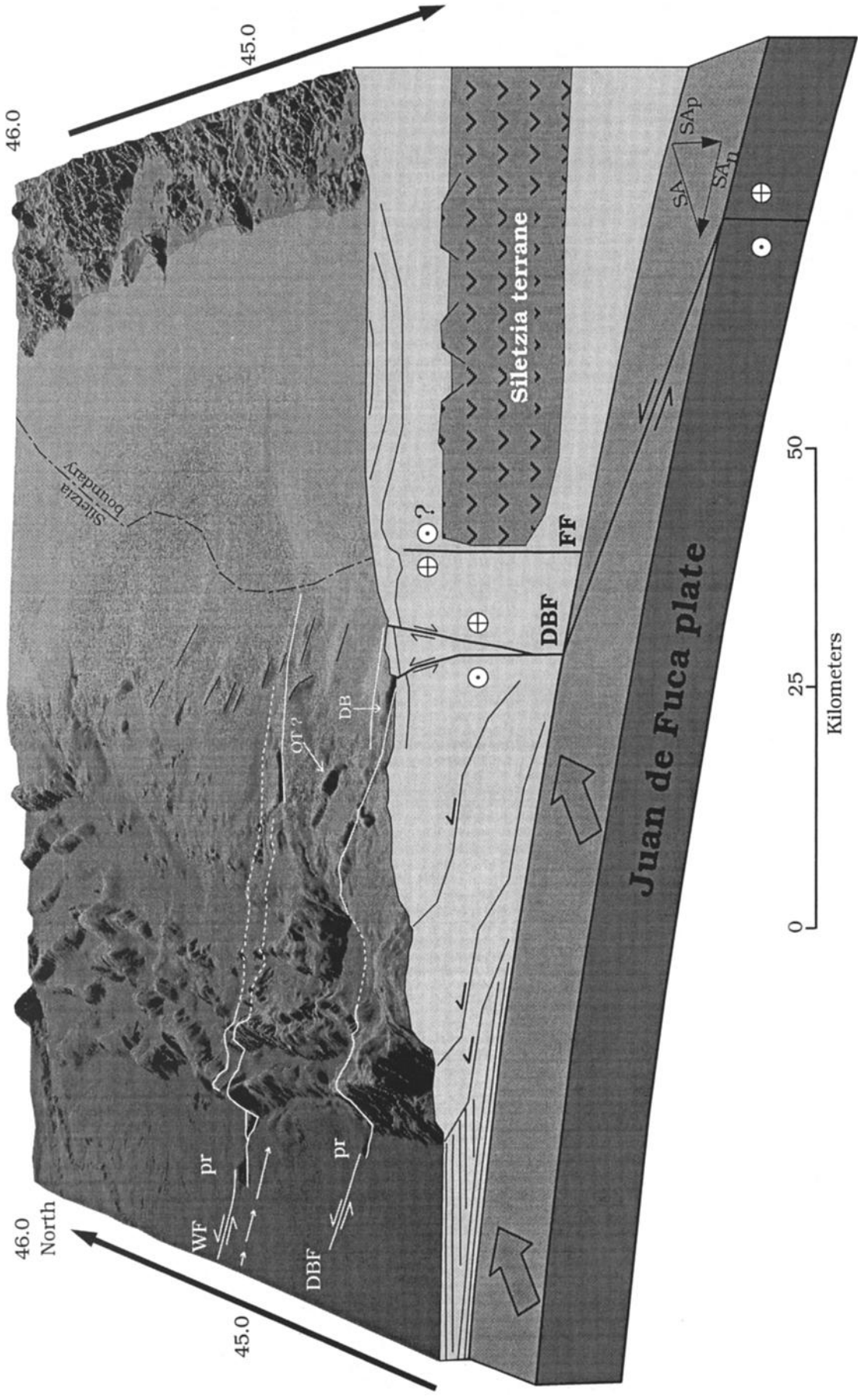
46.0
45.0
Siletzia terrane
Siletzia boundary
SAp
SA
SAn
DBF
FF
?
DB
QT ?
pr
pr
WF
DBF
46.0
North
45.0
Juan de Fuca plate
0
25
50
Kilometers

isopach plots of two abyssal plain stratigraphic units, shows that slip increases landward along the fault from its western tip to the frontal thrust (Figure 15), landward of which isopaching was not possible [*Goldfinger et al.*, 1996a]. The observed decrease in morphological expression across the plate boundary, where slip is still increasing in lower plate units, is most consistent with the fault propagating upward across the poorly coupled décollement. Alternatively, older episodes of slip may be preserved at the landward ends of the faults but may be overprinted by compressional deformation on the lower slope.

We infer that the significant deformation of the accretionary wedge is the expression of faulting originating in the subducting plate, transmitted to a passively deforming upper plate. The passage of the basement faults beneath the accretionary wedge should leave older fault traces that may be progressively overprinted by compressional deformation (Figure 15). The four faults without lower plate expression, as well as other transverse folds and linear features we have observed in SeaBeam bathymetry, may be such older traces. What mechanisms might be responsible for transverse rupture of the subducting slab? Three models that might explain slab rupture are interplate coupling stresses, membrane strain due to slab geometry, and slab stresses imposed by slab-mantle interaction. These models are discussed below.

Origin of the Transverse Faults

Given the evidence for deformation of both plates, in which plate did the deformation originate? *Wang et al.* [1995] calculate that interplate stresses <10 MPa result from JDF plate subduction, consistent with low observed stress drops in subduction earthquakes, assuming that stress release is close to complete [e.g., *Kanamori*, 1980; *Magee and Zoback*, 1993]. High heat flow in Cascadia places the downdip brittle ductile transition for crustal rocks in the outer-shelf-upper slope region [*Hyndman and Wang*, 1995]. Between the poorly coupled accretionary wedge and the shallow brittle ductile transition may be a very narrow zone of significant interplate frictional stress (C. Goldfinger, manuscript in preparation, 1996). We estimate that this narrow zone of coupling is unlikely to be responsible for rupture of the oceanic lithosphere, which has a shear strength, for any conditions of temperature and pore pressure within the brittle regime, greater [e.g., *Brace and Kohlstedt*, 1980] than the interplate coupling stresses inferred by *Wang et al.* [1995].

Another possible scenario for intraslab deformation could be the introduction of membrane strain due to the concave seaward geometry of the Cascadia subduction zone off Washington. This geometry is inferred to result in arching of the slab beneath Washington, with a more steeply dipping slab both to the north and to the south [*Michaelson and Weaver*, 1986; *Crosson and Owens*, 1987]. This slab configuration results in strike-parallel membrane strain as modeled by *Creager et al.* [1995, Figure 3] for the Bolivian syntaxis. Subduction of the JDF slab is expected to result in similar N-S compression, and this model is supported by sparse focal mechanisms [*Spence*, 1989]. A strike-slip focal mechanism indicating right-lateral slip on a NW striking plane or left slip on a NE striking plane is located 30 km seaward of the western tip of the Daisy Bank fault (Figure 2) [*Spence*, 1989]. Either nodal plane for this event is consistent with N-S compression; however, N-S compression in the slab is inconsistent with the nearby WNW striking left-lateral faults. These faults should be dextral if they are driven by N-S compression. The evidence for N-S compression just seaward of the left-lateral faults, though sketchy, suggests that the principal horizontal stress direction is significantly different seaward of the plate boundary than in the subducting slab and suggests to us that membrane strain due to subduction geometry or other mechanisms may be operative but that it must be overprinted by some other mechanism that drives the sinistral transverse faults.

Recently, *Scholz and Campos* [1995] proposed a dynamic model of interplate coupling and decoupling at subduction zones that incorporates the hydrodynamic resistance of the motion of the slab through the viscous mantle. In their model, the mantle is considered stationary in a hot spot reference frame. This "sea anchor" force, in a mantle system that is fixed to the hot spot frame, should have trench-parallel and trench-normal components in the case of oblique subduction [*Scholz and Campos*, Figure 1] (Figure 15). The trench-parallel component of hydrodynamic mantle resistance to subduction is an unbalanced force that sets up a shear couple in the plane of the slab. For Cascadia, the shear couple would be dextral, and antithetic shears should be left-lateral and east-west to northwest trending. We propose that this shear couple may be responsible for the observed transverse rupture of the slab we have observed in the central Cascadia forearc. Limited slab seismicity is consistent with a model of transverse shearing in the subducting slab. The largest instrumentally recorded earthquake in Cascadia (1949, m_b = 7.1; 47.13°N, 122.95°W [*Baker and Langston*, 1987]) occurred in the Puget Sound region in Washington (Figure 2) at a depth of 54 km in the upper part of the subducting plate (Figure 2) [*Baker and Langston*, 1987; *Ludwin et al.*, 1991]. The focal mechanism

Figure 15. Block rotation model for the central Cascadia forearc. SeaBeam bathymetry shaded from the north. The Wecoma and Daisy Bank faults are shown, with the Daisy Bank fault exposed in foreground. Well-mapped fault traces are in solid; discontinuous traces are dashed. The arc-parallel component of oblique subduction creates a dextral shear couple, which is accommodated by WNW trending left-lateral strike-slip faults. We propose that shearing of the slab due to oblique subduction is responsible for the faults involving oceanic crust. "Sea anchor" force and components shown at lower right [*Scholz and Campos*, 1995]. WF, Wecoma fault; DBF, Daisy Bank fault; FF, Fulmar fault; "pr", pressure ridge; "DB", Daisy Bank. "OT?", possible old left-lateral fault strand. Arrow heads and tails show strike-slip motion. White arrows at western end of Wecoma fault show eastward increasing slip calculated from isopach offsets [*Goldfinger et al.*, 1996a]. Dots at eastern end of Wecoma fault indicate the location of the faults shown on Figure 11. Schematic block rotation model shown at lower left, showing deformation of parallelogram ABCD in dextral simple shear [after *Wells and Coe*, 1985].

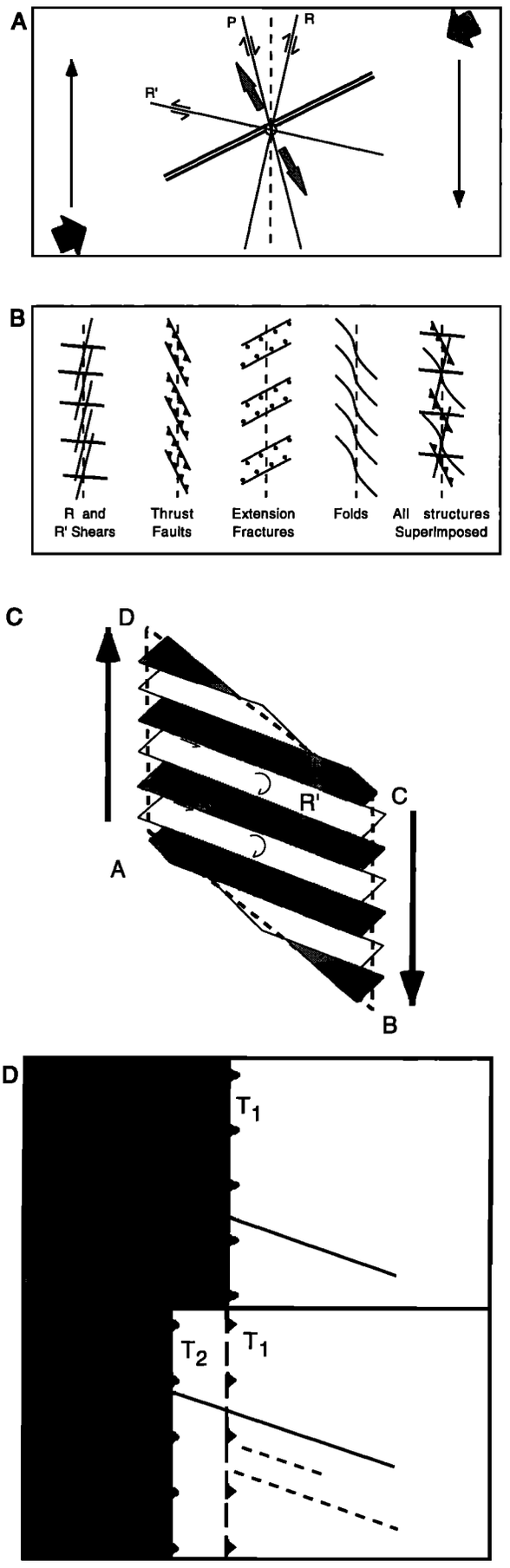

is strike-slip with a preferred fault plane striking east-west ± 15° (azimuth 255-285°) and has nearly pure left-lateral slip [*Baker and Langston*, 1987]. While this strike-slip mechanism indicates shearing within the Juan de Fuca plate, the fault planes of the 1949 event are not parallel to the convergence direction, negating a possible tear fault origin [*Weaver and Baker*, 1988]. A similar left-lateral strike-slip solution was determined for a small 1981 earthquake (magnitude 3.3) in the upper Juan de Fuca plate on the southern Washington coast (Figure 2) [*Taber and Smith*, 1985; *Weaver and Baker*, 1988]. The seismicity plotted on Figure 2 reveals several other interesting patterns. The Washington coast strike-slip event lies at the eastern end of an east-west linear trend of earthquakes that lie roughly on the projection of the South Nitinat fault, and are near a major east-west reverse fault mapped on the shelf. Two events plot near the Wecoma fault, and several plot near the landward end of the Alvin Canyon and Willapa Canyon faults. The depths and locations of all of these events, however, are suspect due to poor azimuthal station coverage (R. Ludwin, personal communication, 1995).

Could the basement involved faults be reactivated structures in the oceanic basalt? Comparison of the strikes of the oblique faults to the seafloor magnetic anomaly map of *Wilson* [1993] shows that the three Washington faults, with strikes of about 283°, could be reactivated small fracture zones perpendicular to the magnetic anomalies. The Oregon faults strike 292° to 325°, deviating from an orthogonal to the magnetic lineations by 12° to 45° and thus are unlikely to be related to preexisting basement structure. We have also considered conjugate shortening of the forearc of the type described by *Lewis et al.* [1988]; however, extensive mapping of margin structures [*Wagner et al.*, 1986; *Clarke*, 1990; *Goldfinger et al.*, 1992a; C. Goldfinger and L. McNeill, manuscript in preparation, 1996] has not identified structures conjugate to the WNW faults. We have mapped two major NE trending structures, one on the slope off northern Oregon and one off central Washington, but both of these are clearly left-lateral tear faults of the accretionary fold-thrust belt.

Kinematic Model: Upper Plate Deformation

Northeasterly directed subduction results in a dextral shear couple in the North American plate and, as suggested above, possibly in the Juan de Fuca plate as well (Figures 15 and 16).

Figure 16. Strike-slip models, convergence shown at 062° for central Oregon using pole of *DeMets et al.* [1990]. (a) Simple shear model showing R, R', and P shears. (b) Structure types and orientations expected in overall right simple shear [after *Sylvester*, 1988]. (c) Block rotation model in a dextral shear couple [after *Wells and Coe*, 1985] (d) Map view interaction of basement strike-slip fault with a growing accretionary wedge. Shading indicates lower plate; no shading indicates upper plate. (top) Time 1, (bottom) time 2. Remanent traces, shown dashed, may remain as active structures or be overprinted by compressional deformation. As the basement fault moves, the accretionary wedge advances, maintaining the youth of the intersection point.

The existence of active sinistral faults in the upper plate, both related and unrelated to basement faulting, suggests that the North American plate may be responding to both passive strain transmitted from the slab and to dextral shear imparted by interplate coupling. In the following discussion we present a model for deformation of the upper plate, which is observable, but a similar model may also be operative in the subducting slab.

Pure shear deformation of the Cascadia margin is well expressed in the fold and thrust belt of the accretionary wedge. For the most part, these structures are subparallel to the margin and represent the response of the upper plate to the normal component of plate convergence. In model experiments of simple shear and in earthquake ground ruptures, five sets of fractures have been observed: R and P or synthetic shears, with the same motion sense as the simple shear couple; R' or antithetic shears, with a motion sense opposite to the main shear; tension fractures or normal faults oriented at about 45° to the main shear zone; and Y shears or faults parallel to the shear couple. Strike-slip, reverse, and normal faults of the orientations shown in Figure 16b are consistent with a simple shear model of overall right-oblique shear [e.g., *Wilcox et al.*, 1973; *Sylvester*, 1988, and references therein], although none of the experimental models involved subduction-driven simple shear. Comparison of the right simple shear model (Figure 16) with the structural map of the Oregon-Washington margin in Figure 2 suggests that the WNW left-lateral faults are consistent with R' shears antithetic to the right shear couple driven by oblique subduction. WNW to NW trending folds and thrust faults of the middle continental slope to outer continental shelf are also expected in the right simple shear model. Y shears, or faults parallel to the main shear couple, would be difficult to detect within the similarly oriented structural grain of the accretionary wedge. We note that the three best mapped fault zones that cross the deformation front, the North Nitinat, Wecoma, and Daisy Bank faults, bend 3-6° southward on the continental slope from their abyssal plain strike (Table 1). The south bending of these two fault zones could be due either to passage of the basement faults beneath the wedge (Figure 16d) or a component of dextral arc-parallel shear distributed across the accretionary wedge, similar to that suggested for the onshore forearc by *England and Wells* (1991).

In the case of the forearc rotation we propose, the shear couple is set up by oblique insertion of the subducted plate into the mantle, and thus two margin-parallel faults may not be required. Linkage between the upper and lower plate faults for anything but a very short time requires slip along the inboard edge of the rotated terrane in the upper plate. *Tréhu et al.* (1995) suggest that a small fault observed to overlie the edge of the Siletzia terrane in central Oregon may represent an active dextral fault that decouples the active wedge from the inboard Siletzia terrane. Our data are somewhat supportive of this hypothesis. We observe a vertical, probably strike-slip fault (eastern fault in Figure 11) that also overlies the edge of the Siletzia terrane (see Figure 2 for location). SeaMARC 1A data show this fault to be NW trending, and we initially correlated it as the northern strand of the Wecoma fault. Alternatively, it could be the same fault shown by *Tréhu et al.* [1995], 7 km to the south. SeaBeam bathymetry reveals that the edge of the Siletzia terrane is overlain by a north trending zone of short, doubly plunging en echelon folds suggestive of

Table 1. Fault Parameters for Oregon-Washington Transverse Strike-Slip Faults

Fault	Strike JDF	Strike NOAM	Net Slip JDF, km	H-LP Slip Rate, mm/yr	Slip Rate, mm/yr	Arc-Parallel Slip, mm/yr	Age, ka	Total Length, km	Length JDF, km	Dip Slip, N. block up, m	Dip, deg., Direction
North Nitnat	282°	288°	2.2 ± 0.3	8.3 ± 4.0	5.5 ± 2	1.2	400 ± 50	115	20	-100	85-90, North
South Nitnat	283°	283°?	2.0 ± 0.8	?	6.7 ± 3	1.5	300 ± 40	> 59	19	-80	85-90, North
Willapa Canyon	N/A	280°	?	?	?	?	?	40	N/A	?	?
Wecoma	292°	296°	5.5 ± 0.8	8.5 ± 4	8.5 ± 2	3.2	650 ± 50	95	21	-100	85-90, North
Daisy Bank	291°	296°	2.2 ± 0.5	?	5.7 ± 2	2.1	380 ± 50	94	21	-70	85-90, North
Alvin Canyon	289°	289°?	2.2 ± 0.5	?	6.2 ± 2	2.5	380 ± 50	64 ?	7	-50	85-90, North
Heceta South	N/A	310° avg.	?	?	?	?	?	35	N/A	?	?
Coos Basin	N/A	290°	?	?	?	?	?	35	N/A	?	?
Thompson Ridge	N/A	301°	?	?	?	?	?	41	N/A	?	?

H-LP, Holocene-late Pleistocene; JDF, Juan de Fuca; NOAM, North America; N/A, not applicable; ?, uncertain; avg., average.

dextral shear at depth (shown on SeaBeam bathymetry in Figure 15)

A geometric requirement of a set of parallel strike-slip faults with the same motion sense is that the intervening blocks and the faults themselves must rotate (Figure 16) [e.g., *Freund*, 1974]. We infer that the Cascadia left-slip faults segment much of the continental slope in Oregon and Washington into elongate blocks rotating clockwise about vertical axes. This style of deformation has been proposed for the Aleutian forearc on a much larger scale [*Geist et al.*, 1988; *Ryan and Scholl*, 1993] and has been documented in other tectonic environments [e.g., *Cowan et al.*, 1986; *Beck*, 1989; *Garfunkel*, 1989; *Jackson and Molnar*, 1990]. Although Cascadia lacks seismicity-defined blocks, paleomagnetically determined clockwise rotation of basalts in western Oregon and Washington indicates that clockwise rotation has occurred throughout most of the Tertiary. A smooth coastward increase in the rotation of the Miocene Gingko and Pomona members of the CRBG is consistent with a model of distributed deformation of the forearc and inconsistent with microplate docking models [*England and Wells*, 1991]. The viscous sheet deformation model of *England and Wells* [1991] implies a northward transport of the forearc at 13-15 mm/yr since the Miocene, or about 75% of the present margin-parallel plate convergence. Such northward transport of the forearc is consistent with our simple shear model.

A block rotation model implies geometric space problems at the margins of the rotated blocks. If the pivots are fixed to the North American plate, compression between the blocks is required. Such compression is observed along the Wecoma, Daisy Bank, Alvin Canyon, and Thompson Ridge faults off Oregon but not along the Washington faults. Without compression along the block edges, the blocks must translate northward relative to the North American plate. Small gaps and overlaps occur at the ends of the blocks (Figure 16). On the abyssal plain, compression is taken up by anticlines and horsetail splays near the western tips of the Wecoma, Daisy Bank, and Alvin Canyon fault and by splays at the North and South Nitinat faults. At the landward block ends, the complexity of the accretionary wedge is such that minor deformation such as this would be difficult to discern.

The fact that five of the nine mapped faults cross the plate boundary must be reconciled with northeasterly subduction at 40 mm/yr. The JDF plate should have traveled 10 to 24 km to the northeast relative to the North American plate during the 0.3 to 0.6 Ma elapsed since the initiation of left-lateral faulting (Table 1). Thus we might expect to observe horizontal offsets of the strike-slip faults where they cross the deformation front, but we have observed few such offsets. We suggest that the interaction between the oblique faults and the growing accretionary wedge tends to reduce the amount of lateral offset expected at the deformation front (Figure 16d). If the deformation front was fixed in east-west position during the known life span of the faults, the expected northward offset across the plate boundary due to northeasterly plate motion would be 4-11 km. *Goldfinger et al.* [1996b] estimate that the deformation front advanced 14-21 km westward during this period based on the age of uplift of thrust ridges [*Kulm et al., 1973a*]. The rapid advance of the deformation front implies that the point of intersection between the strike-slip faults and the frontal thrust is always very young, reducing the expected offset of the frontal thrust. Some possible minor offsets may be interpreted in Figure 5. Nevertheless, the small offsets of the frontal thrust and the relatively straight trends of the fault zones across the slope suggest that the accretionary wedge and subducting plate are not converging along the expected JDF-NOAM plate vector. The forearc may deforming internally and/or translating northward due to oblique subduction [*Pezzopane and Weldon*, 1991; *Wells and Weaver*, 1992; *McCaffrey and Goldfinger*, 1995]. Alternatively, subduction has ceased or dramatically slowed within the last 0.6 Ma. The latter hypothesis conflicts with abundant evidence for modern subduction including Holocene shortening of the accretionary wedge apparent in numerous seismic reflection records throughout the Cascadia margin; onshore geodetic data indicating shortening approximately in the convergence direction [*Savage and Lisowski*, 1991; *Dragert et al.*, 1994]; and paleoseismologic evidence of large, probably subduction-related earthquakes in the coastal bays of Oregon, Washington, and California (e.g., *Atwater*, 1987, 1992; *Darienzo and Peterson*, 1990; *Nelson et al.*, 1995).

The continuity of the oblique strike-slip faults across the plate boundary and the evidence that subduction has occurred through the Holocene to the present suggest to us that the submarine forearc is translating northward, either as a microplate or in small block translations and or rotations. The extensive internal deformation of the forearc supports the latter hypothesis. We find support for northward translation in the active structures of offshore Washington. Structural trends of late Quaternary folds and thrust faults off western Washington are nearly north-south on the continental shelf (Figure 2) [*Wagner et al.*, 1986; C. Goldfinger and L. McNeill, manuscript in preparation, 1996], and are parallel to the margin (~ 020°) on the continental slope. Contemporary fold and thrust trends in the Juan de Fuca Strait, between Washington and Vancouver Island, strike NW, parallel to the strait. Active shortening is apparently occurring across the strait, in contrast to the east-west shortening occurring west of Washington, suggesting that the Washington forearc is colliding with a more rigid Vancouver Island buttress, as suggested by *Wells and Weaver* [1992].

Goldfinger [1994] and *McCaffrey and Goldfinger* [1995] calculated the total rate of forearc deformation in the arc-parallel direction as a result of slip on the nine strike-slip faults (Table 1). A component of extension between points on any two blocks occurs as a result of left-lateral motion on the intervening strike-slip fault. Slip on all nine faults translates the northern end of the rotated domain northward by the sum of these arc-parallel components relative to the southern end, assuming no shortening across the blocks. The net arc-parallel extension rate is 10.5 mm/yr from the five faults with known slip rates. If we assign the lowest known slip rate value, 5.5 mm/yr, to the faults with unknown slip rates, the extension rate is 17.4 mm/yr, or 87% of the 20 mm/yr tangential component of convergence [*Goldfinger*, 1994; *McCaffrey and Goldfinger*, 1995]. If correct, this implies that the oblique faults alone can account for most of the oblique component of subduction. Forearc deformation rates have recently been linked to subduction earthquake magnitude [*McCaffrey*, 1993]. Using the observed difference between subduction earthquake slip vectors and plate motions to estimate total rates of forearc deformation, *McCaffrey* [1993] finds a negative correlation between rapidly deforming forearcs and the largest subduction earthquakes. The physical explanation for this is that earthquake magnitude is ultimately linked to the ability of the forearc to store elastic strain

energy; thus weak forearcs generate smaller earthquakes [*McCaffrey*, 1993]. *McCaffrey and Goldfinger* [1995] calculate that the extensive strike-slip faulting in the central Cascadia forearc may limit subduction earthquakes to about MW 8.0.

Last, the process of block rotation of the Cascadia submarine forearc may have occurred for a longer period of time than the ages of the dated faults. We speculate that new oblique faults periodically rupture the lower plate, and sometimes both plates, then slip for a relatively short period of time, perhaps taking advantage of basement weaknesses. Motion on individual faults may cease after a short period of time, after which the abyssal plain fault traces would be subducted or accreted, depending on the local vergence direction and décollement position. Accreted upper plate faults may remain as active deformation zones or may be altered by mass wasting, deposition, erosion, or subsequent accretionary wedge faulting. In SeaBeam bathymetry and GLORIA sidescan data we have observed many poorly defined WNW trending lineations that may be the remnants of previous episodes of strike-slip faulting, one of which is shown on Figure 15. Alternatively, if the faults are no older than the dated growth strata on the abyssal plain, the observed deformation could be very young, reducing the effect of JDF motion on the time history of upper plate deformation.

Conclusions

Using sidescan sonar, seismic reflection profiles, and swath bathymetric data, we have mapped a set of WNW trending left-lateral strike-slip faults that deform the Oregon and Washington submarine forearc. Evidence for left-lateral separation includes offset of accretionary wedge folds, channels, and other surficial features; sigmoidal left bending of accretionary wedge folds; and offset of abyssal plain sedimentary units. Five of these faults cross the plate boundary, extending 5-21 km into the Juan de Fuca plate. Using offset of subsurface piercing points and offset of approximately dated submarine channels, we calculate slip rates for these five faults of 5.5 to 8.5 mm/yr. Little or no offset of these faults by the basal thrust of the accretionary wedge is observed. Holocene offset of submarine channels and unconsolidated sediments is observed in sidescan records and directly by submersible.

The strike-slip faults are most likely driven by dextral shearing of the subducting slab and propagate upward through the overlying accretionary wedge. Tangential hydrodynamic drag caused by oblique insertion of the slab into the mantle is a possible driving mechanism. Four sinistral faults observed in only the upper plate may be remanent traces of previous basement-driven deformation. Alternatively, a similar, though unrelated dextral shear couple driven by interplate coupling may drive these faults and may augment deformation of the upper plate for all the sinistral faults.

A model of overall right-lateral simple shear of the submarine forearc is consistent with the observed surface faults, which may be R' or antithetic shears to the overall right-shear couple. The major strike-slip faults define elongate blocks that, because of their orientation and sinistral slip direction, must rotate clockwise. We infer that the deformation of the submarine forearc (defined to include the lower plate) is highly strain-partitioned into arc-normal shortening and arc-parallel strike-slip and translation. The high slip rates of the strike-slip faults, coupled with the lack of offset of these faults as they cross the plate boundary, imply that the seaward accretionary wedge is not moving at the expected convergence rate relative to the subducting plate. We conclude that the accretionary wedge is rotating and translating northward, driven by the tangential component of Juan de Fuca-North American plate convergence.

Acknowledgments. We thank the crews of the research vessels *Thomas Thompson* (University of Washington), and support vessels *Cavalier* and *Jolly Roger*; *Delta* pilots Rich and Dave Slater, Chris Ijames, and Don Tondrow; members of the Scientific Party on cruises from 1992 to 1993 during which most of the data were collected; Kevin Redman, David Wilson, Tim McGiness, Wolf Krieger, Chris Center, and Kirk O'Donnell from Williamson and Associates of Seattle Washington, our sidescan contractors; Ed Llewellyn for co-writing *Sonar*, OSU's sidescan-sonar processing software; and Chris Fox, and Steve Mutula of NOAA for their assistance with the multibeam data. Multibeam bathymetry data were collected by NOAA and processed by the NOAA Pacific Marine and Environmental Laboratory, Newport Oregon. Thanks to Chris Fox and Bob Dziak, also of NOAA Newport, Oregon for the T wave earthquake locations shown in Figure 2. We thank Eric Geist, Roger Bilham, and Greg Moore for thorough and helpful reviews. This research was supported by National Science Foundation grants OCE-8812731 and OCE-9216880; U.S. Geological Survey National Earthquake Hazards Reduction Program awards 14-08-0001-G1800, 1434-93-G-2319, and 1434-93-G-2489; and the NOAA Undersea Research Program at the West Coast National Undersea Research at the University of Alaska grants UAF-92-0061 and UAF-93-0035.

References

Appelgate, T. B., C. Goldfinger, L. D. Kulm, M. MacKay, C. G. Fox, R. W. Embley, and P. J. Meis, A left-lateral strike-slip fault seaward of the central Oregon convergent margin, *Tectonics, 11*, 465-477, 1992.

Atwater, B. F., Evidence for great Holocene earthquakes along the outer coast of Washington State, *Science, 236*, 942-944, 1987.

Atwater, B. F., Geologic evidence for earthquakes during the past 2000 years along the Copalis River, southern coastal Washington, *J. Geophys. Res., 97*, 1901-1919, 1992.

Baker, G. E., and C. A. Langston, Source parameters of the 1949 magnitude 7.1 South Puget Sound, Washington, earthquake as determined from long-period body waves and strong ground motions, *Bull. Seismol. Soc. Am., 77*, 1530-1557, 1987.

Barnard, W. D., The Washington continental slope: Quaternary tectonics and sedimentation, *Mar. Geol., 27*, 79-114, 1978.

Beck, M. E., Jr., On the mechanism of tectonic transport in zones of oblique subduction, *Tectonophysics, 93*, 1-11, 1983.

Beck, M. E. Jr., Block rotations in continental crust: examples from North America, in *Paleomagnetic Rotations and Continental Deformation*, edited by C. Kissel, and C. Laj, pp. 1-16, Kluwer Acad. Norwell, Mass., 1989.

Bilham, R., and P. Bodin, Fault zone connectivity: slip rates on faults in the San Francisco Bay area, California, *Science, 258*, 281-284, 1992.

Blake, M. C., D. C. Engebretson, A. S. Jayko, and D. L. Jones, Tectonostratigraphic terranes in southwest Oregon, in *Tectonostratigraphic Terranes of the Circum-Pacific Region*, edited by D. G. Howell, pp. 147-157, Circum-Pac. Counc. for Energy and Miner. Resour., Houston, Tex., 1985.

Brace, W. F., and D. L. Kohlstedt, Limits on lithospheric stress imposed by laboratory experiments, *J. Geophys. Res., 85*, 6248-6252, 1980.

Carson, B., E. Seke, V. Paskevich, and M. L. Holmes, Fluid expulsion sites on the Cascadia accretionary prism: Mapping diagenetic deposits with processed GLORIA imagery, *J. Geophys. Res., 99*, 11,959-11,969, 1994.

Clarke, S. H., Jr., Map showing geologic structures of the northern California continental margin, scale 1:250,000, *U.S. Geol. Surv. Map, MF-2130*, 1990.

Cowan, D. S., M. Botros, and H. P. Johnson, Bookshelf tectonics: Rotated crustal blocks within the Sovanco Fracture Zone, *Geophys. Res. Lett., 13*, 995-998, 1986.

Cranswick, D. J., and K. A. Piper, Geologic framework of the Washington-Oregon continental shelf-Preliminary findings, in *Proceedings of the 1991 Exclusive Economic Zone Symposium on Mapping and Research: Working Together in the Pacific EEZ, U.S. Geol. Surv. Circ. 1092*, p. 146-151, 1992.

Creager, K. C., L. Y. Chiao, J. P. Winchester, and E. R. Engdahl, Membrane strain rates in the subducting plate beneath South America, *Geophys. Res. Lett., 22*, 2321-2324, 1995.

Crosson, R. S., and T. J. Owens, Slab geometry of the Cascadia subduction zone beneath Washington from earthquake hypocenters and teleseismic converted waves, *Geophys. Res. Lett., 14*, 824-827, 1987.

Darienzo, M. E., and C. D. Peterson, Episodic tectonic subsidence of late Holocene salt marshes, northern Oregon central Cascadia margin, *Tectonics, 9*, 1-22, 1990.

Davis, D., J. Suppe, and F. A. Dahlen, Mechanics of fold-and-thrust belts and accretionary wedges, *J. Geophys. Res., 88*, 1153-1172, 1983.

DeMets, C., R. G. Gordon, D. F. Argus, and S. Stein, Current plate motions, *Geophys. J. Int., 101*, 425-478, 1990.

Dewey, J. F., and S. H. Lamb, Active tectonics of the Andes, *Tectonophysics, 205*, 79-95, 1992.

Dragert, H., R. D. Hyndman, G. C. Rogers, and K. Wang, Current deformation and the width of the seismogenic zone of the northern Cascadia subduction thrust, *J. Geophys. Res., 99*, 653-658, 1994.

EEZ-SCAN 84 Scientific Staff, Atlas of the exclusive economic zone, western conterminous United States, scale 1:500,000, *U. S. Geol. Surv., Misc. Invest. Ser.*, I-1972, 1986.

England, P., and R. E. Wells, Neogene rotations and quasicontinuous deformation of the Pacific northwest continental margin, *Geology, 19*, 978-981, 1991.

Fitch, T. J., Plate convergence, transcurrent faults, and internal deformation adjacent to southeast Asia and the western Pacific, *J. Geophys. Res., 77*, 4432-4460, 1972.

Freund, R., Kinematics of transform and transcurrent faults, *Tectonophysics, 21*, 93-134, 1974.

Garfunkel, Z., Regional deformation by block translation and rotation, in *Paleomagnetic Rotations and Continental Deformation*, edited by C. Kissel and C. Laj, *NATO ASI Ser. C, 254*, 181-208, 1989.

Geist, E. L., J. R. Childs, and D. W. Scholl, The origin of summit basins of the Aleutian Ridge: Implications for block rotation of the arc massif, *Tectonics, 7*, 327-341, 1988.

Goldfinger, C., Active deformation of the Cascadia forearc: Implications for great earthquake potential in Oregon and Washington, Ph.D. thesis, Oreg. State Univ., Corvallis, 1994.

Goldfinger, C., and L. C. McNeill, Case study of GIS data integration and visualization in submarine tectonic investigations: Cascadia subduction zone, *Mar. Geod.* in press, 1996.

Goldfinger, C., L. D. Kulm, and R. S. Yeats, Neotectonic map of the Oregon continental margin and adjacent abyssal plain, scale 1:500,000, *Open File Rep. O-92-4*, Oreg. Dep. of Geol. and Miner. Ind., Portland, 1992a.

Goldfinger, C., L. D. Kulm, R. S. Yeats, B. Appelgate, M. MacKay, and G. F. Moore, Transverse structural trends along the Oregon convergent margin: Implications for Cascadia earthquake potential, *Geology, 20*, 141-144, 1992b.

Goldfinger, C., L. D. Kulm, R. S. Yeats, B. Appelgate, M. MacKay, and G. R. Cochrane, Active strike-slip faulting and folding of the Cascadia plate boundary and forearc in central and northern Oregon, in *Assessing and Reducing Earthquake Hazards in the Pacific Northwest*, edited by A. M. Rogers, T. J. Walsh, W. J. Kockelman, and G. Priest,, *U.S. Geol. Surv. Prof. Pap., 1560*, p. 223-256 1996a.

Goldfinger, C., L. D. Kulm, R. S. Yeats, C. Hummon, G. J. Huftile, A. R. Niem, and L. C. McNeill, Oblique strike-slip faulting of the Cascadia submarine forearc: The Daisy Bank fault zone off central Oregon, in *Subduction: Top to Bottom, Geophys. Monogr. Ser.*, vol. 96, edited by G.E. Bebout et al., pp. 65-74, AGU, Washington, D.C., 1996b.

Griggs, G. B., and L. D. Kulm, Origin and development of Cascadia deep-sea channel, *J. Geophys. Res., 78*, 6325-6339, 1973.

Harding, T. P., and J. D. Lowell, Structural styles, their plate-tectonic habitats, and hydrocarbon traps in petroleum provinces, *AAPG Bull., 63*, 1016-1058, 1979.

Hyndman, R. D., and E. E. Davis, A mechanism for the formation of methane hydrate and seafloor bottom simulating reflectors by vertical fluid expulsion, *J. Geophys. Res., 97*, 7025-7041, 1992.

Hyndman, R. D., and K. Wang, The rupture zone of Cascadia great earthquakes from current deformation and the thermal regime, *J. Geophys, Res., 100*, 22,133-22,154, 1995.

Jackson, J., and P. Molnar, Active faulting and block rotations in the western Transverse Ranges, California, *J. Geophys. Res., 95*, 22,073-22,087, 1990.

Jarrard, R. D., Terrane motion by strike-slip faulting of forearc slivers, *Geology, 14*, 780-783, 1986.

Kanamori, H., State of stress in the Earth's lithosphere, in *Proceedings of the 1979 Enrico Fermi Summer School, Varenna, Italy, Physics of the Earth's Interior*, pp. 551-553, edited by A. M. Dziewonski and E. Boschi, North-Holland, New York, 1980.

Karig, D. E., D. R. Sarewitz, and G. D. Haeck, Role of strike-slip faulting in the evolution of allochthonous terranes in the Philippines, *Geology, 14*, 852-855, 1986.

Kelsey, H. M., and J. G. Bockheim, Coastal landscape evolution as a function of eustasy and surface uplift rate, Cascadia margin, southern Oregon, *Geol. Soc. Am. Bull.*, 106, 840-854, 1994.

Kimura, G., Oblique subduction and collision: Forearc tectonics of the Kuril arc, *Geology, 14*, 404-407, 1986.

Kimura, G., S. Maruyama, Y. Isozaki, and M. Terabayashi, Well-preserved underplating structure of the jadeitized Franciscan complex, Pacheco Pass, California, *Geology, 24*, 75-78, 1996.

Kulm, L. D., and G. A. Fowler, Oregon continental margin structure and stratigraphy: A test of the imbricate thrust model, in *The Geology of Continental Margins*, edited by C. A. Burke and C. L. Drake, pp. 261-284, Springer-Verlag, New York, 1974.

Kulm, L. D., and E. Suess, Relation of carbonate deposits and fluid venting, Oregon accretionary prism, *J. Geophys. Res., 95*, 8899-8915, 1990.

Kulm, L. D. et al., Site 174, *Initial Rep. Deep Sea Drill. Proj., 18*, 97-167, 1973a.

Kulm, L. D., R. A. Prince, and P. D. Snavely Jr., Site Survey of the northern Oregon continental margin and Astoria Fan, *Initial Rep. Deep Sea Drill. Proj., 18*, 979-987, 1973b.

Lewis, S. D., J. W. Ladd, and T R. Bruns, Structural development of an accretionary prism by thrust and strike-slip faulting: Shumagin region, Aleutian Trench, *Geol. Soc. Am. Bull., 100*, 767-782, 1988.

Ludwin, R. S., C. S. Weaver, and R. S. Crosson, Seismicity of Washington and Oregon, in *Neotectonics of North America*, DNAG CSMV-1, edited by D. B. Slemmons, E. R. Engdahl, D. Blackwell, and D. Schwartz, pp. 77-98, Geol. Soc. of Am., Boulder, Colo., 1991.

MacKay, M. E., Structural variation and landward vergence at the toe of the Oregon accretionary prism, *Tectonics, 14*, 1309-1320, 1995.

MacKay, M. E., G. F. Moore, G. R. Cochrane, J. C. Moore, and L. D. Kulm, Landward vergence and oblique structural trends in the Oregon margin accretionary prism: Implications and effect on fluid flow, *Earth Planet. Sci. Lett., 109*, 477-491, 1992.

Magee, M. E., and M. D. Zoback, Evidence for a weak interplate thrust fault along the northern Japan subduction zone and implications for the mechanics of thrust faulting and fluid expulsion, *Geology, 21*, 809-812, 1993.

McCaffrey, R., Slip vectors and stretching of the Sumatran forearc, *Geology, 19*, 881-884, 1991.

McCaffrey, R., On the role of the upper plate in great subduction zone earthquakes, *J. Geophys, Res., 98*, 11,953-11,966, 1993.

McCaffrey, R., and C. Goldfinger, Forearc deformation and great earthquakes: Implications for Cascadia earthquake potential, *Science, 267*, 856-859, 1995.

Michaelson, C. A., and C. S. Weaver, Upper mantle structure from teleseismic *P* wave arrivals in Washington and northern Oregon, *J. Geophys. Res., 91*, 2077-2094, 1986.

Moore, J. C., G. F. Moore, G. R. Cochrane, and H. J. Tobin, Negative-polarity seismic reflections along faults of the Oregon accretionary

prism: Indicators of overpressuring, *J. Geophys. Res., 100*, 12,895-12,906, 1995a.

Moore, J. C. et al., Abnormal fluid pressures and fault-zone dilation in the Barbados accretionary prism: Evidence from logging while drilling, *Geology, 23*, 605-608, 1995b.

Nelson, A. R. et al., Radiocarbon evidence for extensive plate-boundary rupture about 300 years ago at the Cascadia subduction zone, *Nature, 378*, 371-374, 1995.

Nelson, C. H., Marine geology of the Astoria deep-sea fan, Ph.D. dissertation, 287pp., Oreg. State Univ., Corvallis, 1968.

Niem, A. R., N. S. MacLeod, J. Snavley, P. D., D. Huggins, J. D. Fortier, H. J. Meyer, A. Seeling, and W. A. Niem, Onshore-offshore geologic cross section, northern Oregon Coast Range to continental slope, *Oreg. Dep. Geol. Miner. Ind., Spec. Pap.* 26, 10pp, 1992.

Pezzopane, S. K., and R. J. Weldon II, Tectonic role of Holocene fault activity in Oregon, *Tectonics, 12*, 1140-1169, 1991.

Rohr, K. M., and K. P. Furlong, Ephemeral plate tectonics at the Queen Charlotte triple junction, *Geology, 23*, 1035-1038, 1995.

Ryan, H. F., and D. W. Scholl, Geologic implications of great interplate earthquakes along the Aleutian arc, *J. Geophys. Res., 98*, 22,135-22,146, 1993.

Sangawa, A., A history of fault movement since late Pliocene in the central part of southwest Japan, *Bull. R. Soc. N. Z., 24*, 75-85, 1986.

Savage, J. C., and M. Lisowski, Strain measurements and potential for a great subduction earthquake off the coast of Washington, *Science, 252*, 101-103, 1991.

Scholz, C., and J. Campos, On the mechanism of seismic decoupling and back arc spreading at subduction zones, *J. Geophys. Res, 100*, 22,103-22,115, 1995.

Scholz, C. H., N. H. Dawers, J.-Z. Yu, and M. H. Anders, Fault growth and fault scaling laws: Preliminary results, *J. Geophys. Res., 98*, 21,951-21,961, 1993.

Seely, D. R., The significance of landward vergence and oblique structural trends on trench inner slopes, in *Island Arcs, Deep Sea Trenches and Back-Arc Basins, Maurice Ewing Ser.* vol. 1, edited by M. Talwani and W.C. Pitman, pp. 187-198, AGU, Washington, D.C., 1977.

Shipboard Scientific Party, Site 892, in G.K. Westbrook, B. Carson, R. J. Musgrove,et al., *Proc. Ocean Drill. Program, Initial Rep., part 1*, 146,: College Station, TX (Ocean Drilling Program), 234-300, 1994.

Snavely, P. D., Jr., Tertiary geologic framework, neotectonics, and petroleum potential of the Oregon-Washington continental margin, in *Geology and Resource Potential of the Continental Margin of Western North America and Adjacent Ocean Basins-Beaufort Sea to Baja California*, edited by D. W. Scholl, A. Grantz, and J. G. Vedder, pp. 305-335, Circum-Pac. Counc. for Energy and Miner. Resour., Houston, Tex., 1987.

Spence, W., Stress origins and earthquake potential in Cascadia, *J. Geophys. Res., 94*, 3076-3088, 1989.

Sternberg, R. W., Transport and accumulation of river-derived sediment on the Washington continental shelf, *J. Geol. Soc. London, 143*, 945-956, 1986.

Sylvester, A. G., Strike-slip faults, *Geol. Soc. Am. Bull., 100*, 1666-1703, 1988.

Taber, J. J., Jr., and S. W. Smith, Seismicity and focal mechanisms associated with the subduction of the Juan de Fuca plate beneath the Olympic Peninsula, Washington, *Bull. Seismol. Soc. Am., 75*, 237-249, 1985.

Tobin, H. J., J. C. Moore, M. E. MacKay, D. L. Orange, and L. D. Kulm, Fluid flow along a strike-slip fault at the toe of the Oregon accretionary prism: Implications for the geometry of frontal accretion, *Geol. Soc. Am. Bull., 105*, 569-582, 1993.

Tréhu, A., G. Lin, E. Maxwell, and C. Goldfinger, A seismic reflection profile across the Cascadia subduction zone offshore central Oregon: New constraints on methane distribution and crustal structure, *J. Geophys. Res., 100*, 15,101-15,116, 1995.

Wagner, H. C., L. D. Batatian, T. M. Lambert, and J. H. Tomson, Preliminary geologic framework studies showing bathymetry, locations of geophysical tracklines and exploratory wells, sea floor geology and deeper geologic structures, magnetic contours, and inferred thickness of Tertiary rocks on the continental shelf and upper continental slope of southwest Washington between latitudes 46°N and 48° 30'N and from the Washington coast to 125° 30'W, *Open File Rep. 86-1*, 10 pp., Wash. Div. of Geol. and Earth Resour., Olympia, 1986.

Wang, K., T. Mulder, G. C. Rogers, and R. D. Hyndman, Case for very low coupling stress on the Cascadia subduction fault, *J. Geophys. Res., 100*, 12,907-12,918, 1995.

Weaver, C. S., and G. E. Baker, Geometry of the Juan de Fuca plate beneath Washington and northern Oregon from seismicity, *Bull. Seismol. Soc. Am., 78*, 264-275, 1988.

Weaver, C. S., and S. M. Smith, Regional tectonic and earthquake hazard implications of a crustal fault zone in southwestern Washington, *J. Geophys. Res., 88*, 10,371-10,383, 1983.

Wells, R. E., and R. S. Coe, Paleomagnetism and geology of Eocene volcanic rocks of southwest Washington, implications for mechanisms of tectonic rotation, *J. Geophys. Res., 90*, 1925-1947, 1985.

Wells, R. E., and P. L. Heller, The relative contribution of accretion, shear, and extension to Cenozoic tectonic rotation in the Pacific Northwest, *Geol. Soc. Am. Bull., 100*, 325-338, 1988.

Wells, R. E., and C. S. Weaver, Rotating crustal blocks and big earthquakes in western Oregon and Washington, *Geol. Soc. Am. Abstr. Programs, 24*, 89, 1992.

Wilcox, R. E., T. P. Harding, and D. R. Seely, Basic wrench tectonics, *Am. Assoc. Pet. Geol. Bull., 57*, 74-60, 1973.

Wilson, D. S., Confidence intervals for motion and feformation of the Juan de Fuca Plate, *J. Geophys. Res., 98*, 16,053-16,071, 1993.

C. Goldfinger and L. D. Kulm, College of Oceanic and Atmospheric Sciences, Oregon State University, Corvallis, OR 97331. (email: gold@oce.orst.edu; lkulm@oce.orst.edu)

C. Hummon, L. McNeill, and R. S. Yeats, Department of Geosciences, Oregon State University, Corvallis, OR 97331. (email: hummonc@ucs.orst.edu; lmcneill@oce.orst.edu; yeatsr@bcc.orst.edu)

(Received February 13, 1996; revised August 23, 1996;
accepted August 28, 1996.)